Signal distortion and scattering losses in on-chip plasmonic communication

Ashfaq Ahmad

Department of Electronics

Quaid-i-Azam University, Islamabad
Pakistan

A Thesis Submitted in Partial Fulfillment of the Requirements
for the Degree of

Doctor of Philosophy
in
Electronics

August, 2024

QUAID-I-AZAM UNIVERSITY
Department of Electronics

Author's Declaration

I, **Ashfaq Ahmad** hereby state that my PhD thesis titled **"Signal Distortion and Scattering Losses in on-chip Plasmonic Communication"** is my own work and has not been submitted previously by me for taking degree from **Department of Electronics, Quaid-i-Azam University** Or anywhere else in the country/world.

At any time if my statement is found to be incorrect even after my graduation, the university has the right to withdraw my PhD degree.

Mr. Ashfaq Ahmad

Date: _____

QUAID-I-AZAM UNIVERSITY
Department of Electronics

Plagiarism Undertaking

I solemnly declare that research work presented in the thesis titled, "Signal Distortion and Scattering Losses in on-chip Plasmonic Communication" is solely my research work with no significant contribution from any other person. Small contribution/help wherever taken has been duly acknowledged and that complete thesis has been written by me.

I understand the zero-tolerance policy of the HEC and Quaid-i-Azam University towards plagiarism. Therefore, I as an Author of the above titled thesis, declare that no portion of my thesis has been plagiarized and any material used as reference is properly referred/cited.

I undertake that if I am found guilty of any formal plagiarism in the above titled thesis even after award of PhD degree, the University reserves the rights to withdraw/revoke my PhD degree and that HEC and the University has the right to publish my name on the HEC/University Website on which names of students are placed who submitted plagiarized thesis.

Student/Author Signature: _____

Name: **Mr. Ashfaq Ahmad**

QUAID-I-AZAM UNIVERSITY
Department of Electronics

Certificate of Approval

This is to certify that the research work presented in this thesis, entitled "**Signal Distortion and Scattering Losses in on-chip Plasmonic Communication**" was conducted by **Mr. Ashfaq Ahmad** under the supervision of **Dr. Muhammad Arshad Fiaz**. No part of this thesis has been submitted anywhere else for any other degree. This thesis is submitted to the **Department of Electronics, Quaid-i-Azam University** in partial fulfilment of the requirements for the degree of Doctor of Philosophy in Field of **Electronics,** Department of Electronics, Quaid-i-Azam University.

Student Name: **Mr. Ashfaq Ahmad**   Signature: _____

Examination Committee:

A. Dr. Khurram Saleem Alimgeer   Signature: _____
   Associate Professor, Senior Incharge,
   Electrical Engineering Department,
   COMSATS University, Park Road, Chak Shahzad,
   Islamabad.

B. Dr. Abdullah Waqas   Signature: _____
   Assistant Professor
   Department of Computer Science,
   National University of Technology
   Islamabad.

C. Dr. Muhammad Arhsad Fiaz (Supervisor) Signature: _____
   Associate Professor
   Department of Electronics
   Quaid-i-Azam University, Islamabad.

D. Prof. Dr. Muhammad Aqueel Ashraf   Signature: _____
   Chairman
   Department of Electronics
   Quaid-i-Azam University, Islamabad

Supervisor Name: **Dr. Muhammad Arshad Fiaz**   Signature: _____

Name of Chairman: **Prof. Dr. Muhammad Aqueel Ashraf** Signature: _____

Dedicated to my parents for their unconditional love, care, and continuous encouragement throughout my life and to my supervisor Dr. Muhammad Arshad Fiaz for his continuous encouragement, support, and intuitive guidance.

Acknowledgements

Abstract

The enhancement of scattered field from cylindrical structures in the presence of surface plasmon polariton (SPP) waves is analyzed. The SPP waves are excited using the Turbadar-Kretschmann-Raether (TKR) configuration and a cylindrical wave approach (CWA) is implemented to obtain the scattered field. Different arrangements such as a corner reflector and a strip are simulated by means of multiple metallic circular scatterers. It is noted that the back-scattered field from the strip is very strong and can be one of the main challenges in plasmonic communication. Moreover, the simulations give the idea that what combination of structure size and distance from the interface does not produce significant scattering for both the strip and corner reflector. To better understand the phenomenon, and to provide a good insight, two-dimensional near zone field maps are generated to observe field in the vicinity of the object. In the presence of SPP waves, simulations show strong field near the edges like dipole field which is contrary to usual scattering in the absence of SPP waves for a plane wave illumination.

In a second problem, scattering of SPP waves excited by a sinusoidal grating from a metallic circular scatterer is described. The extended boundary condition method (EBCM) is utilized to derive the reflectance and transmittance. The angles of exciting SPP (θ_{SPP}) are measured by analyzing the behavior of reflectance.

Numerical results are reported for different values of the size and distance of scatterer from the grating. It has been observed that the scattered field increases as the size of the scatterer increases. Additionally, the scattered field intensity is much higher when the

angle of the incident is equal to the angle of SPP wave excitation ($\theta_i = \theta_{SPP}$) than when the angle of the incident is not θ_{SPP}.

The scattered field reduces as the distance of the scatterer from the grating increases, which shows that the effect of SPP waves near the interface is much stronger than away from the interface. Additionally, the effect of the period and height of the grating on the scattered field are also analyzed. By increasing the period from 900 nm to 1700 nm, the position and the width of the peaks change. It has been noticed that the scattered field increases with an increase in the height of the grating.

From the above analysis, it is evident that the signal propagation will be interrupted by the presence of a strong scattered field. Interference of SPP wave propagation with scattered fields is quite obvious. Moreover, the reception of SPP scattering at the receiver is another factor that will distort the information sent to the receiver. The simulated scenarios help in determining the combination of size and distance which does not distort the signal propagation due to scattering effects. This simulation gives an idea of how far an object should be in order to avoid scattering effects in plasmonic communication. It can be deduced that the scattering effect can be neglected for the SPP wave propagation when the distance of the object is $h = 100\ nm$ with size $R = 5\ nm$.

List of Publications

The following is a list of publications in refereed journals, produced during this Ph.D. candidature.

1. **Ashfaq Ahmad**, et al. Enhanced Scattering from Cylindrical Structures in the Presence of SPP Waves. *Plasmonics,* vol. 19, pp. 1951–1960, 2024.

2. **Ashfaq Ahmad**, and Muhammad Arshad Fiaz, Scattered field from a PEMC cylinder buried below rough interface using extended boundary condition method, *Optik,* vol. 193, pp. 162572, 2019.

3. **Ashfaq Ahmad**, and Muhammad Arshad Fiaz, Near zone scattering and extinction properties of a left handed material cylinder buried in a semi infinite medium with rough interface. *Journal of Modern Optics,* vol. 66, no. 12, pp. 1358-1368, 2019.

4. Abdullah Khalid, **Ashfaq Ahmad**, and Muhammad Arshad Fiaz. Scattered field from a single/double negative grounded slab with rough interface. *Optik,* vol. 208, pp. 164484, 2020.

Contents

List of Figures

List of Tables

Chapter 1

Introduction

Communication relies heavily on electronics which makes it possible to achieve miniaturization and device integration. Power efficiency and information processing speed are the other attractive features. The desired high data rate requires high frequency pulse propagation. Consequently, high thermal noise becomes a challenging issue as described by Plank's law. Moreover, the distortion in pulse shape and power loss in interconnects between electronic chip components are other factors that make the scenario worse during signal transmission. It is a fact that electronics have reached the lower bound on size imposed by the diffraction limit and further miniaturization is not possible. Also, a further high data rate cannot be achieved. Miniaturization causes an increase in resistance (R) while the capacitance (c) remains almost the same [1]. This increase results in high RC delay.

Photonics seems promising in terms of the high data rate utilizing the optical fiber with negligibly small scattering and dissipative losses. It is easy to achieve integration with existing on-chip electrical communication systems. However, optical devices are not small enough on a wavelength scale. Moreover, the compact integration of many functions in a single device, like an electronic analog is difficult to realize. Optical fibers are substantially larger than the nano-electronic devices of today, with sizes in the hundreds of nanometer range. Both electronics and photonics are facing limitations in the growing efforts to transfer massive amounts of data at high speeds while trying to achieve miniaturization in size. Because of their disparate capacities and sizes, it is

challenging to integrate them to achieve a high bit rate and downsizing. The difficulty in confining light into small dimensions (diffraction limit) compared to the wavelength is the main factor for this bottleneck [2].

The critical dimensions of different chip-scale device technologies and operating speeds are given in figure (1.1). Modern electronics works very well in miniaturization. The critical dimensions of the devices can be downsized below 10 *nm* and they can be large up to 1 *um*. The maximum speed that can be achieved is GHz and cannot be exceeded due to the RC delay issue. To overcome these issues, photonics are introduced. The maximum speed is raised to THz. Miniaturization is not possible below 1 *um* which is the critical limit of photonic devices and also called the diffraction limit. The limitations being faced by electronics and photonics can be addressed by plasmonics. Plasmonics can operate at a THz speed similar to that of photonics and can be miniaturized at the nanoscale similar to electronics. Due to these qualities, plasmonics seems very promising in future communication.
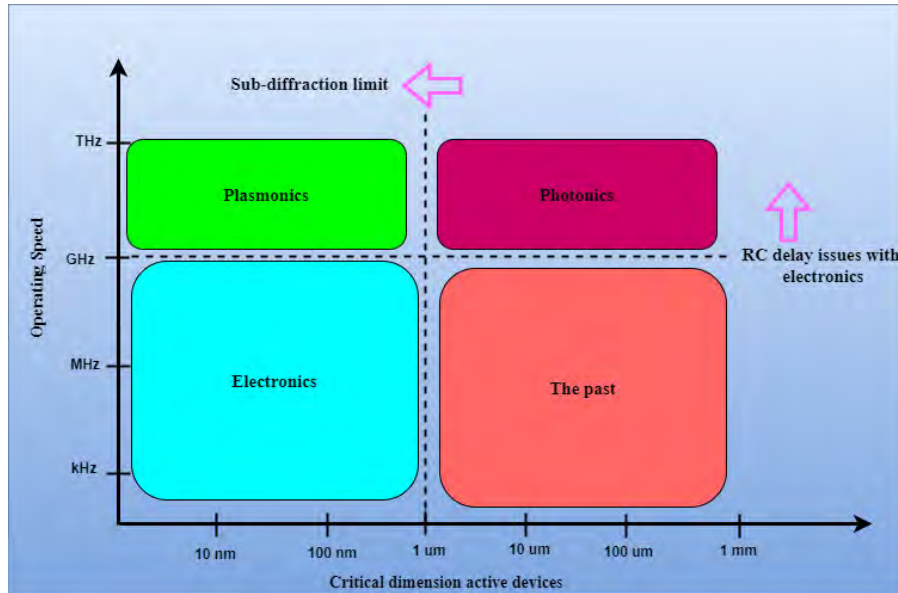
Figure 1.1: Relation between dimensions and data speed for the operating regimes of different available communication technologies.

1.1   Plasmonic communication

Plasmonics can do miracles in designing a communication device with a limit less than the limit of diffraction imposed by nature. The next breakthrough in telecommunications, computing, imaging, etc., can only emerge with advances in plasmonics. The merging of electronics and photonics can be achieved by using plasmonics. The future of wave communication is believed to be plasmonics. One of the main merits of plasmonics in communication is the confinement of light waves on metal dimensions below the diffraction limit. A plasmon is the quantum of the plasma oscillation. Plasmonics is the analysis of the electron cloud oscillation in metals and semiconductors in response to irradiated light [3]. Plasmonics finds wide-ranging applications in various domains, including devices for clocking [4, 5], spectroscopy [6, 7], cancer therapy [8], and nanosensing [9–11].

Plasmonics can be characterized by two main components: surface plasmon polaritons (SPPs) and localized surface plasmons (LSPs) [12]. SPP is associated with surface charge oscillation. Surface plasmon expresses a charge motion in the metal, while polaritons describe electromagnetic waves in a dielectric medium. SPPs are the surface waves that propagate along the metal dielectric interfaces. These waves are formed by coupling photons with the collective oscillations of free electrons at the metal surface. They are envisioned as one of the most combative prospects for next-generation information carriers because of their tight spatial confinements and strong local field intensities. These characteristics of SPPs make them particularly attractive for next-generation information carriers.

On-chip optical communications and computation represent a highly anticipated future for ultra-fast communication and high-speed data processing [13]. This technology holds substantial promise for addressing the limitations encountered in traditional electronic systems. Therefore, SPPs have already attracted a lot of research attention in the last couple of decades, and a variety of structures have been designed and proposed to guide and regulate them [14–22]. SPPs have garnered significant research attention over the past few decades, leading to the design and proposal of various structures intended to

guide, manipulate, and control their behavior. A multitude of structures and methodologies have been developed to regulate SPPs. As a result, the creation of novel optical technologies for communication is improving, and academics are becoming increasingly interested in this sector. The field of optical communication technologies is evolving rapidly, and numerous advancements are being made, resulting in growing attention and enthusiasm among academia.

SPP waves have a number of applications, including solar photovoltaics [23–25], on-chip optical computing [26], communications [27–29], and optical sensing [30–32]. SPP pulse can be sent and received with less energy required than a metallic wire. Because of these special characteristics, plasmons can travel at a high bit rate across nanoscale interconnects (wires) that carry information in microprocessors. Plasmonic interconnects [33] play a key role in chip design because they facilitate the rapid development of smaller and faster transistors, which in turn speed up data transfer throughout the device. Moreover, a waveguide based on plasmon not only guides the light at nanoscales but also works as a path to integrate the devices on a chip [34].

Scientists are interested in the application of plasmonics in communication. The main objective is to develop novel optical systems and components that are comparable in size to the tiniest integrated circuits and components. Afterward, plasmonic data creation, transport, and detection are future tasks by integrating the components into an electronic chip. It is possible to build plasmon generators [35], detectors [36], cables [37], splitters [38], and even plasmonsters [39]. The primary focus of applications is on managing the expenses and losses associated with nanofabrication processes. A pure plasmonic circuit for communication consists of a light source, a collimator [40], a waveguide [41–44], and switches [45, 46].

Zhang et al. [47] proposed a nano-scale laser that consists of a wire made of cadmium sulphide. It is placed on a silver surface with an insulating gap of 5 nm. It has been coated with magnesium fluoride. The wire's length and width are in micrometers and nanometers, respectively. A light having a wavelength of 405 nm is targeted on the nanowire. A photon is emitted from the wire causing SPPs, which bounce back and forth between its ends. These plasmons excite atoms in cadmium sulphide to emit laser light of a

wavelength of 489 *nm*. For a similar wavelength, the diameter is about 245 *nm* less than that of a conventional laser. Plasmonic collimation gives an efficient coupling between laser and waveguide. The high-directional emission from sub-wavelength apertures encircled by surface wrinkles serves as the basis for the plasmonic collimator. A lot of interest is being shown in plasmonic waveguides that operate across the spectrum, ranging from visible to the far infrared. For plasmonics waveguides, a number of metrics have been proposed and examined, including propagation distance, confinement mode, quality factor, group velocity, and distance from the light line. A plasmonic circuit requires plasmonic switches. In the literature, various types of plasmonic switches are discussed. Recent technological developments have made it possible the plasmonic nanocircuits which leads to data generation, transmission, and detection at the plasmonic level [48–52]. Plasmonic nanocircuits are engineered structures that leverage the unique properties of plasmonic waves for manipulating and transmitting data at the nanoscale. At frequencies of order tens of GHz, usual cables suffer from ohmic losses, while plasmonic transmission losses are small. Thus, long-distance communications using plasmonic transmission is achieved [53].

In addition to many advantages, a few challenges require attention. SPP wave applications in on-chip communications may suffer from scattering losses during signal transmission, resulting in power loss and pulse shape distortion. These losses can lead to adverse effects such as power reduction and distortion of the pulse shape, impacting the overall integrity and strength of the transmitted signals. In order to build plasmonic communication applications, it is critical to first understand the scattering mechanisms and properties [54]. This knowledge is essential for comprehending how SPPs interact with structures, materials, and imperfections, affecting their behavior during communication. This thesis focuses on investigating the scattering of SPP waves from multiple canonical objects such as strip, ring, and corner reflector which are made of metallic circular scatterers, and their effects on plasmonics communication and SPP wave propagation. The analysis of the scattered field is done both in the presence and absence of SPP waves. The analysis of the scattered field in both the presence and absence of SPP waves is a critical approach for un-

derstanding the behavior and characteristics of these waves when interacting with various structures or objects.

To the best of our knowledge, scattering of SPP waves from cylindrical structures simulated by multiple cylinders has not been reported. The simulation of SPP wave scattering from cylindrical structures using multiple cylinders remains insufficiently explored or documented in the existing literature. This indicates a potential research gap or an area that isn't extensively explored or addressed within the context of SPP wave simulations. The absence of documented studies exploring the scattering of SPP waves from cylindrical structures simulated by multiple metallic circular scatterers could present an opportunity for future research and investigation in the field of plasmonics and nanophotonics.

1.2 Two-dimensional scattering

Scattering is a phenomenon where a portion of the power of a propagating electromagnetic (EM) wave is redirected as secondary EM waves in different directions, deviating from the original direction of propagation. There are several scattering processes, which are usually classified in terms of the size of the scattering particles in relation to the wavelength of the scattered light, such as Rayleigh scattering, Mie scattering, and Raman scattering, etc.

In Rayleigh scattering [55], the size of the scattering particles or the scale of inhomogeneities in a medium is much smaller than the wavelength of light approximately $\lambda/10$. In response to incident light the dielectric particles become polarized. The field induces dipole oscillations in the particle, leading to the emission of EM waves in multiple directions. The intensity of the scattered light is $I \propto 1/\lambda^4$. It can be deduced that a short wavelength will scatter more than a large wavelength. The scattering of blue light with a 0.4 µm wavelength is 16 times greater than that of red light with a 0.8 µm wavelength.

When the dimensions of the scatterers are comparable to or greater than the wavelength of the incident light, it is unequivocally described by Mie theory or Mie scattering [56]. Rayleigh scattering occurs in all directions, while Mie scattering is most prominent in the forward direction. The scattering depends

on the relationship between the size of the scattering particle and the wavelength of light, favoring scattering in a forward direction. The dependency of the wavelength is less pronounced in comparison to Rayleigh scattering. Mie scattering creates a whitish glare around the sun in the presence of a high amount of particulate matter in the air. It also gives white light from the mist and fog.

Similarly, when a photon is incident on the molecules the energy is either gained or lost, and the frequency of the scattered photon is shifted, such inelastic scattering is called Raman scattering [57]. The photon emitted from the laser excites the atoms in molecules. These excited electrons are in a virtual state. In this state, electrons are not stable so they fall to the ground state immediately. As a result, photons are emitted. There are three different scenarios of how light can be remitted after energy has been absorbed by an electron, i.e., Rayleigh scattering, Stokes Raman scattering, and anti-Stokes Raman scattering. If the energy of the scattered photon is the same as that of the incident photon, this is called Rayleigh scattering. In addition, when the scattered photon has less energy than the incident photon is known as Stokes Raman scattering. Similarly, Anti-Stokes Raman scattering occurs when the scattered photon has energy higher than the incident photon.

A signal may deteriorate during propagation due to dispersion, absorption, and scattering losses in the presence of impurities and obstacles. Scattering occurs due to the roughness of interfaces and the curviness of objects. The phenomenon can be categorized into scattering from objects and scattering from rough interfaces. Moreover, surfaces can be characterized as flat surface, slightly rough surface and rough surface. Reflection and transmission by a flat surface in specular direction can be found in many textbooks [58, 59]. Extension to this problem has been done to design waveguides [60], fiber optics [61], binoculars [62] etc. Scattering from a slightly rough surface is widely discussed in the literature. Generally, perturbation theory (PT) is used to study scattering from slightly rough surface having small height as well as small slope [63, 64]. A detailed study on the validity of the PT is presented by Crespo *et al.* [65]. Guo *et al.* [66] discussed the scattering from conducting rough surface using high order small perturbation method with tapered incidence field. Bi-static

scattering from dielectric structures with two rough boundaries using the perturbation theory (PT) is presented in [67]. PT was also used to study a perfect electromagnetic conductor (PEMC) rough surface [68, 69].

In addition to the slightly rough surface, large roughness is widely discussed in the literature. An extended form of SPM is the extended boundary condition method (EBCM) which is applied to periodic surfaces by many authors. Waterman [70] used it to study scattering from sinusoidal surface. Comparison of EBCM with other methods such as a method of moments (MOM), and modified physical Optics (MPO) is reported by Chuang, *et al.* [71]. Results show good agreements with experimental data obtained at optical frequencies when the complex permittivity of the metal grating is considered. Guidance by dielectric waveguide with periodic surfaces is studied in [72]. Comparison of results with experimental data is done for metallic gratings with surface plasmon excitations. Tsang, *et al.* [73] provided complete details for EBCM. It is well known fact that matrix ill-conditions are observed when the surface groove is deep or when the ratio of corrugations depth and surface period is large. A solution is reported in [74].

The EBCM uses algebraic equations in matrix form to calculate the amplitudes of scattered fields related to the amplitude of the incident field [70]. According to this method, the radiated field from the induced currents on the surface should cancel the incident field everywhere below the surface, which is derived from Green's theorem. Applying to the dielectric surface the tangential fields above the dielectric surface produce a field that can exactly cancel the incident field at any point below the surface, while a reflected field exists in the region above the surface. Through boundary conditions, the tangential field component below is related to the field above the surface. This leads to the transmitted field and is a result of Huygens' principle. Similarly, the dipole field generated in a dielectric medium can be represented as a combination of two waves, explained by the extinction theorem [75, 76]. One of these waves nullifies the incident wave entirely, while the other wave travels through the dielectric medium. The method's simplicity allows it to tackle more challenging problems, such as conical diffraction [77] and the scattering of acoustic waves from a periodic surface that is either fluid or solid [78].

1.2.1 Cylindrical wave approach (CWA)

The second category involves scattering from objects either metallic or dielectric. The investigation of plane wave scattering in the literature is a well-studied and extensive subject, with various researchers employing diverse techniques to understand and analyze this phenomenon. Scattering from a metallic object has widely been investigated in literature considering the shape either spherical or cylindrical [79]. The object of an arbitrary cross section is also studied [80]. Solution to the problem is more advantageous when the object placed near an interface is assumed. It can solved by applying Green's method [81]. An iterative method based on calculating successive reflections from the interface using a spectral representation of the field is applied to visualize the scattering properties. Full wave solution incorporating all the multiple interactions is also formulated which is known as the cylindrical wave approach (CWA). The CWA is one of the methods used to investigate the scattering from the cylindrical objects [82–85]. This method is utilized to study and analyze the scattering of electromagnetic waves from cylindrical objects. This approach permits an understanding of how cylindrical structures interact with incident waves and how the scattered waves propagate.

The CWA is an effective method in the spectral domain for obtaining a detailed solution to 2-D scattering problems [82]. In [83] a technique has been developed to numerically evaluate 2-D diffraction integrals that involve a generic function modulated by a highly oscillating kernel. This approach involves working on the plane wave spectra, considering the multiple interactions of these waves with the interface. It accounts for phenomena such as multiple reflection, transmission, and scattering. The CWA technique is used in [84, 85] for examining the diffraction of a plane wave incident on a metallic cylinder above and below the interface.

One of the notable advantages of this technique is its applicability to arbitrary values of permittivity, size, and location of targets, as well as arbitrary values of the permittivity of the host media, whether lossy or lossless. Scattering from buried targets using CWA is rigorously discussed in the literature [86–89]. The implementation in the spectral domain allows for easy modeling

of dispersive mediums. General-shaped targets can be effectively simulated by approximating them with a suitable set of small circular cylinders. Moreover, this method can be extended to study the propagation of incident pulsed waves with a general shape in the time domain [90, 91].

Scattering from buried objects in a layered medium is addressed in [92–94]. Similarly, the CWA is utilized to observe the scattering of the targets behind a wall [95, 96]. Additionally, a version of CWA has been formulated to account for roughness in the air-soil interface [97, 98].

In the above described scenarios plane wave scattering has been observed. In addition, SPP waves also exhibit scattering from the interfaces. An incident of a single plane wave on the interface between two isotropic media having distinct refractive indices excites two plane waves. One is a reflected wave, while the other is a transmitted wave. In contrast to plane waves, a single SPP wave incident at the interface between two media with different refractive indices, induces a set of scattered plane waves, in addition to reflected and transmitted waves. SPP wave scattering and reflection by surface defects have been analyzed theoretically by many researchers [99–103]. A point-dipole approximation for SPP wave scattering and its limitations are studied for a spherical particle in [104]. It is based on the assumption that the field is constant inside the scatterer. Due to this, the excitation of high order multipole components can be neglected. It has been observed that the differential cross section for SPP-to-SPP scattering is strong in the direction of the SPP wave incident and decreasing with the increase in the distance of particles from the surface. The applicability of this method is discussed in [105]. The scattering properties of particles depend on the shape of the particles [106–108]. SPP wave scattering by a small ellipsoid is described using a point-dipole approximation in [109].

Scattering, reflectivity, and transmission of SPP wave incident on a single and multiple dielectric metallic surfaces are presented in [110]. A surface plasmon distributed Bragg reflector (DBR) model is reported and it may reflect 80% and 90% incident power. A number of surface optical elements such as waveguides, lenses, and reflectors are also designed [111–115]. The performance of these devices is strongly affected by parasitic scattering of SPPs. At a single interface 10% —30% of SPP energy typically scatters into the free space [110].

This phenomenon severely impedes the performance of the surface optical elements and effectively precludes the realization of the 2-D optic paradigm with existing isotropic materials. An anisotropic metamaterial is used to completely eliminate the parasitic scattering [116]. A pathway to plasmonics optics is illustrated by decoupling the response of plasmonic circuits to varying polarization of electromagnetic radiation. Silicon-based plasmonics can shrink the size of the photonic components into sub-wavelength scale [117]. Enhanced detection and emission of optical signals can also be achieved. In this thesis, we apply CWA to study plane wave and SPP wave scattering from a strip and corner reflector. Two configurations known as prism and grating coupled are utilized to excite the SPP waves.

1.3   Objectives and organization of the thesis

The main objective of this dissertation is to study the stimulation of SPP waves. The scattered SPP field is calculated using CWA and their scattering from metallic objects. The dissertation describes how different circular structures scatter SPP waves for experimental purposes. Additionally, it examines how various structural scatterers impact plasmonic communication. How do the different sizes of scatter affect plasmonic communication? Besides, how far an object may be placed in the chip design to avoid the scattering effect. Moreover, how do the period and height of the sinusoidal grating affect the scattering of SPP waves?

In chapter 2, two methods for exciting surface plasmon-polariton (SPP) waves are presented. These methods include prism-coupled and grating-coupled configurations. The chapter also discusses the formulation and numerical results for the Turbadar- Kretschmann- Raether (TKR) configuration. Additionally, it provides the formulation and numerical results for exciting SPP waves through a sinusoidal grating coated with different metals, such as silver, aluminum, and gold.

In chapter 3, the scattering of SPP waves using TKR configuration is presented. We observe the scattering from different structures made from small metallic circular scatterers in the presence and absence of SPP waves. The analytical

formulation and numerical results are reported for various structures made of small circular scatterers, such as corner reflector, strip, etc.

Finally, chapter 4 describes the scattering of SPP waves excited by a sinusoidal grating coupled configuration. The theoretical formulation is presented for a metallic circular scatter. The numerical results have been reported for objects of different sizes, along with the distance of the objects from the grating, the period, and the height of the grating. In conclusion, interference introduced by SPP scattering and signal distortion at the receiver is highlighted.

Chapter 2

Excitation of SPP waves

A photon must have sufficient frequency and momentum to excite a SPP wave. However, a photon in free space at a specific frequency has less momentum than an SPP wave due to the difference in wave vectors described by dispersion relations. This mismatch in momentum is one of the major reasons why photons in free space can't directly couple to the SPP wave.

SPP waves are considered one of the most historical and theoretically analyzed waves among electromagnetic waves [118–120]. The theoretical foundations of SPP waves date back more than a century when Zenneck [121] proposed that electromagnetic waves can propagate along the air-ground interface in the microwave region. Sommerfeld presented a rigorous mathematical analysis of what is termed the Zenneck wave [122]. It is further investigated in several works [123, 124]. Ritchie and Eldridge proposed the concept of Zenneck wave almost 60 years later in the form of SPP wave [125]. It has been analyzed that real components of two different homogeneous dielectric and isotropic materials have opposite signs of relative permittivity [126, 127]. In addition, metal has real negative permittivity [128], while a few other materials are also suitable [129, 130]. Over the years, the theory has evolved to provide further understanding of the interfacing of metal with other complex materials including absorbing crystals [131], semiconductors [132], and anisotropic media [133–137]. The impact of an isotropic and homogeneous dielectric material on the excitation and propagation of SPP waves has been studied. Addition to single mode SPP wave propagation, multi mode SPP wave propagation is also

discussed in [138]. A planar metal interface and a chiral sculptured (STF) thin film has been used. Several studies have been conducted to take into consideration continuously changing materials such as layered structures [139–143] and cholestatic liquid crystals [144, 145]. A commonly used detection technique for biochemical and chemical substances is used based on the polarization of various dielectric materials when electromagnetic field interaction takes place [146, 147].

The canonical boundary-valued problems show that a single SPP wave can propagate if the associated material is homogeneous, isotropic, or dielectric, [126, 127] and [147]. They also reveal which polarization can excite the SPP waves. The same is the case when the interface is made of an anisotropic material. However, the canonical problem reveals that numerous SPP waves with distinct attenuation rates and several phase velocities exist if the related material is dielectric, periodically anisotropic, and homogeneous [148]. The experimental studies on this theoretical concept validate the prediction [149, 150]. In addition, a few studies have also revealed that theoretically and experimentally, s-polarized surface waves can be directed at multilayered dielectric material interfaces with metal [151, 152].

In this chapter, two configurations for exciting SPP waves are discussed. One is the prism-coupled configuration discussed in section (2.1) while the other approach is the grating-coupled configuration in section (2.3). The prism-coupled configuration also known as TKR configuration is based on attenuated total reflection (ATR). The formulation and numerical results are provided in section (2.2) for various values of wavelength and refractive index to calculate the excitation angle of the SPP wave. The grating coupled configuration is based on specular and non-specular reflection from sinusoidal grating coated with a metallic layer. Silver (Al), aluminum (Ag), and gold (Au) have been utilized for coating. The formulation and numerical results for different coated sinusoidal profiles are given to observe the angle of excitation of SPP waves in section (2.4).

2.1   Prism-coupled configuration

The most widely used configuration for exciting the SPP wave uses coupling to the prism through attenuated total reflection (ATR). Figure (2.1a) demonstrates the TKR configuration [153], in which a prism with a high refractive index is coupled to a sufficiently thick dielectric material through a thin metallic layer. In addition, an oil with a refractive index equal to the index of the prism is inserted between the metal and the prism. The oil is used to mitigate air bubbles when light is incident on metal film. A part of the incident light is reflected towards the prism and a part is refracted in the metal surface.

It is worth noting that refracting waves into metal exponentially decays perpendicular to the metal/prism surface. However, if the metallic interface is thin, the wave penetrates from the metal and it further couples to the SPP wave in the metal interface. At a specific angle of incidence to the metal interface and prism, boundary conditions are satisfied to excite the SPP wave at the dielectric and metal interface. A new configuration, termed the Turbadar-Otto (TO) configuration [154] is formed by interchanging metal films and dielectric in the TKR configuration. Figure (2.1b) shows the TO configuration in which the incident field on the prism-dielectric interface is transmitted at an angle greater than the critical angle. In the case that the dielectric film is thin, the phase velocity of an evanescent wave propagating parallel to the interface and the SPP wave propagating along the metallic-dielectric interface are equal.

Note that TKR configuration can only be used to excite SPP waves while TO configuration can also be used to generate Tamm waves or Dyakonov waves in addition to SPP waves if the metal film is regularly changed with an isotropic or anisotropic material that is non-homogeneous. Both the above mentioned prism-coupled configurations are used for stimulating SPP waves with the required polarization state and are easy to implement. However, it is crucial to differentiate between the SPP waves transmitted along the metal-dielectric interface and the waveguide modes propagating within the bulk of the corresponding dielectric material with finite thickness.

(a) TKR configuration   (b) TO configurations
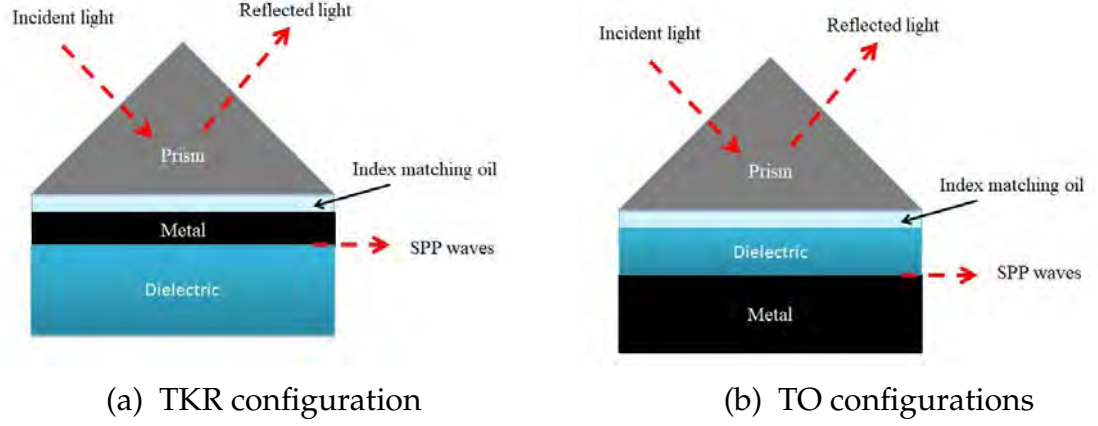
Figure 2.1: Schematic of TKR and TO configurations to excite the SPP waves using prism coupled configuration

2.2 SPP waves excitation using TKR configuration

The geometry of the problem is shown in figure (2.2) similar to the TKR configuration. Medium 1 is considered a high refractive index medium to work as a prism to excite SPP waves, with permittivity of $\epsilon_1 = \epsilon_o\epsilon_{r1}$, while medium 2 is a metallic layer with permittivity of $\epsilon_2 = \epsilon_o\epsilon_{r2}$. The medium 3 has the permittivity of $\epsilon_3 = \epsilon_o$. An $e^{-j\omega t}$ time convention is assumed and suppressed in the formulations, while all the media are considered non-magnetic, homogenous, linear, and isotropic. However most electrical engineering textbooks reference the conventional time-harmonic $e^{+j\omega t}$, but we adopt the unconventional time-harmonic $e^{-j\omega t}$ throughout this thesis. A transverse magnetic polarized wave $\psi(\xi, \zeta) = H_y$ is incident and it may be written as

$$\psi_i(\xi, \zeta) = \psi_0 e^{jn_1(n_\perp^i \xi + n_\parallel^i \zeta)}, \quad \xi < 0 \tag{2.1}$$

The field reflected due to the incident field is

$$\psi_r(\xi, \zeta) = \psi_0 \Gamma_{12}(n_\parallel^i) e^{jn_1(-n_\perp^i \xi + n_\parallel^i \zeta)}, \quad \xi < 0 \tag{2.2}$$
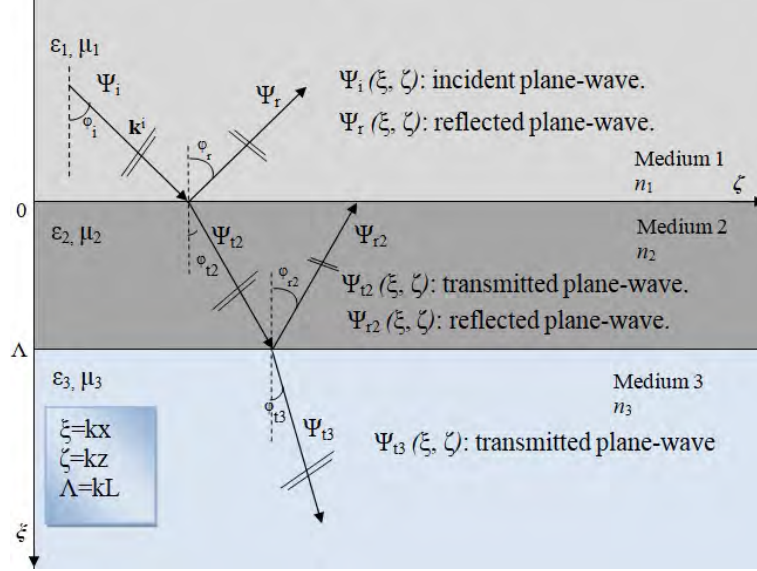
Figure 2.2: Description of field components in prism, metallic layer, and dielectric material for TKR configuration.

The transmitted and reflected fields into the metallic layer are written as

$$\psi_{t2}(\xi,\zeta) = \psi_0 T_{12}(n_\parallel^i)e^{jn_2(n_\perp^{t2}(\xi-\Lambda)+n_\parallel^{t2}\zeta)}, \quad 0 < \xi < \Lambda \tag{2.3}$$

$$\psi_{r2}(\xi,\zeta) = \psi_0 T_{12}(n_\parallel^i)\Gamma_{23}(n_\parallel^i)e^{jn_2(-n_\perp^{t2}(\xi-\Lambda)+n_\parallel^{t2}\zeta)}, \quad 0 < \xi < \Lambda \tag{2.4}$$

The transmitted field can be described as

$$\psi_{t3}(\xi,\zeta) = \psi_0 T_{12}(n_\parallel^i)T_{23}(n_\parallel^i)e^{jn_3(-n_\perp^{t3}(\xi-\Lambda)+n_\parallel^{t3}\zeta)}, \quad \xi > \Lambda \tag{2.5}$$

The corresponding E_y can be computed using Maxwell's equation. Applying the boundary condition at $\xi = 0$, we get.

$$\psi_0 e^{jn_1 n_\parallel^i \zeta} + \psi_0 \Gamma_{12}(n_\parallel^i)e^{jn_1 n_\parallel^i \zeta} = \psi_0 T_{12}(n_\parallel^i)e^{jn_2(n_\perp^{t2}(-\Lambda)+n_\parallel^{t2}\zeta)}$$
$$+\psi_0 T_{12}(n_\parallel^i)\Gamma_{23}(n_\parallel^i)e^{jn_2(-n_\perp^{t2}(-\Lambda)+n_\parallel^{t2}\zeta)} \tag{2.6}$$

$$jn_1 n_\perp^i(\psi_0 e^{jn_1 n_\parallel^i \zeta} + \psi_0 \Gamma_{12}(n_\parallel^i)e^{jn_1 n_\parallel^i \zeta}) = jn_2 n_\perp^{t1}(\psi_0 T_{12}(n_\parallel^i)$$
$$e^{jn_2(n_\perp^{t2}(-\Lambda)+n_\parallel^{t2}\zeta)} + \psi_0 T_{12}(n_\parallel^i)\Gamma_{23}(n_\parallel^i)e^{jn_2(-n_\perp^{t2}(-\Lambda)+n_\parallel^{t2}\zeta)}) \tag{2.7}$$

and at $\xi = \Lambda$

$$\psi_0 T_{12}(n_\parallel^i)e^{jn_2 n_\parallel^{t2}\zeta} + \psi_0 T_{12}(n_\parallel^i)\Gamma_{23}(n_\parallel^i)e^{jn_2 n_\parallel^{t2}\zeta} =$$
$$\psi_0 T_{12}(n_\parallel^i)T_{23}(n_\parallel^i)e^{jn_3 n_\parallel^{t3}\zeta} \tag{2.8}$$

$$jn_2 n_\parallel^{t2}(\psi_0 T_{12}(n_\parallel^i)e^{jn_2 n_\parallel^{t2}\zeta} + \psi_0 T_{12}(n_\parallel^i)\Gamma_{23}(n_\parallel^i)e^{jn_2 n_\parallel^{t2}\zeta}) =$$
$$jn_3 n_\parallel^{t3}(\psi_0 T_{12}(n_\parallel^i)T_{23}(n_\parallel^i)e^{jn_3 n_\parallel^{t3}\zeta}) \tag{2.9}$$

After some algebraic manipulation, reflection and transmission coefficients can be obtained as [155].

$$\Gamma_{12} = \frac{e^{-jn_2 n_\perp^{t2}\Lambda}\left(1 + \frac{n_3 n_\perp^{t3}}{n_2 n_\perp^{t2}}\right)\left(1 - \frac{n_2 n_\perp^{t2}}{n_1 n_\perp^i}\right) - e^{jn_2 n_\perp^{t2}\Lambda}\left(1 - \frac{n_3 n_\perp^{t3}}{n_2 n_\perp^{t2}}\right)\left(1 + \frac{n_2 n_\perp^{t2}}{n_1 n_\perp^i}\right)}{e^{-jn_2 n_\perp^{t2}\Lambda}\left(1 + \frac{n_3 n_\perp^{t3}}{n_2 n_\perp^{t2}}\right)\left(1 + \frac{n_2 n_\perp^{t2}}{n_1 n_\perp^i}\right) + e^{jn_2 n_\perp^{t2}\Lambda}\left(1 - \frac{n_3 n_\perp^{t3}}{n_2 n_\perp^{t2}}\right)\left(1 - \frac{n_2 n_\perp^{t2}}{n_1 n_\perp^i}\right)} \tag{2.10}$$

and

$$T_{12} = \frac{2\left(1 + \frac{n_3 n_\perp^{t3}}{n_2 n_\perp^{t2}}\right)}{e^{-jn_2 n_\perp^{t2}\Lambda}\left(1 + \frac{n_3 n_\perp^{t3}}{n_2 n_\perp^{t2}}\right)\left(1 + \frac{n_2 n_\perp^{t2}}{n_1 n_\perp^i}\right) + e^{jn_2 n_\perp^{t2}\Lambda}\left(1 - \frac{n_3 n_\perp^{t3}}{n_2 n_\perp^{t2}}\right)\left(1 - \frac{n_2 n_\perp^{t2}}{n_1 n_\perp^i}\right)} \tag{2.11}$$

.

2.2.1 Results and discussion

The reflectance and transmittance as a function of the incident angle shown in figure (2.3) are reproduced [54] to determine the excitation angle of SPP wave (θ_{SPP}). The upper layer is a prism having refractive index $n_1 = 2.6$ and the metallic layer is aluminum having refractive index $n_2 = \sqrt{-54 + 21j}$ while the lower layer is air/dielectric having $n_3 = 1$. The thickness of the metallic layer is L = 15 nm, and the wavelength of the incident wave is $\lambda = 633$ nm. Additionally, for further confirmation, there is a 2-D map in figure (2.4) where the field intensity is stronger at the interface and decreases away from it. The

SPP wavevector for a thick metallic film can be expressed as [27]

$$k_{SP} = k_o \sqrt{\frac{\epsilon_2 \epsilon_3}{\epsilon_2 + \epsilon_3}} \tag{2.12}$$

where ϵ_2 and ϵ_3 are the metal and dielectric permittivities respectively while k_o is the wave number of the free space. A transverse magnetic (TM) polarized plane wave incident on a metallic interface from the prism having a wavevector parallel to the interface is [27]

$$k_x = k_o \sqrt{\epsilon_1} \sin(\theta_i) \tag{2.13}$$

where ϵ_1 is the permittivity of the prism and θ_i is the angle of the incident wave. By matching the wavevectors in equations (2.12) and (2.13), we can calculate the angle θ_{SPR}, known as the surface plasmon resonance angle, which excites SPP waves ($\theta_{inc} = \theta_{SPP}$),

$$\theta_{SPP} = \sin^{-1}\left(\frac{1}{\sqrt{\epsilon_1}} \sqrt{\frac{\epsilon_2 \epsilon_3}{\epsilon_2 + \epsilon_3}} \right) \tag{2.14}$$

Using equation (2.14) the angle of excitation of SPP wave is obtained as $22.8140°$ which is very close to $22.9°$ and can be observed in figure (2.3).

In figure (2.5) reflectance as a function of incident angle is plotted for different values of wavelength and refractive index. This figure is dedicated to excite the SPP waves at different angles. From figure (2.5a) it can be observed that excitation occurs at $\theta_{ssp} = 23.07°$ for wavelength $\lambda = 800$ nm, $n_1 = 2.6$, $n_2 = \sqrt{-54 + 21j}$, $n_3 = 1$, and L = 15 nm. The angle of excitation changes to $\theta_{ssp} = 23.35°$ for wavelength $\lambda = 700$ nm, $n_1 = 2.6$, $n_2 = \sqrt{-34 + 13j}$, $n_3 = 1$, and L = 15 nm as presented in figure (2.5b).

It is evident that the angle of excitation can be selected by the wavelength and refractive index of metal. This dependency is further analyzed in figure (2.6) where the angle of excitation of the SPP wave changes from $\theta_{spp} = 25.5°$ to $\theta_{spp} = 24.2°$ as the refractive index and wavelength change. In figure (2.6a), $n_1 = 2.6$, $n_2 = \sqrt{-10 + 13j}$, $n_3 = 1$, L = 15 nm and $\lambda = 500$ nm while in figure (2.6b), $n_1 = 2.6$, $n_2 = \sqrt{-17 + 12j}$, $n_3 = 1$, L = 15 nm and $\lambda = 633$ nm are

used.
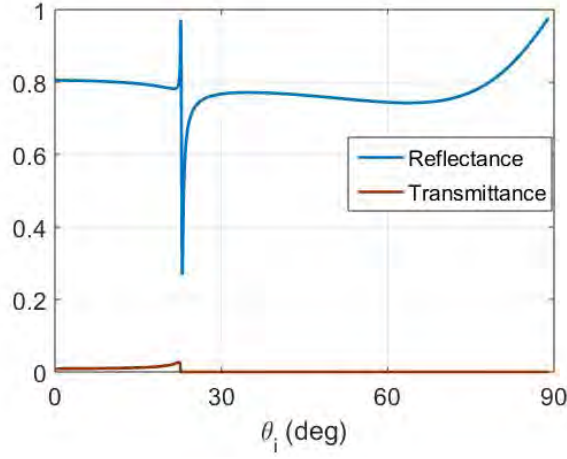
Figure 2.3: Reflectance and transmittance as a function of incident angle, where $n_1 = 2.6$, $n_2 = \sqrt{-54 + 21j}$ and $n_3 = 1$ and L=15 nm while $\lambda = 633$ nm. The dip at angle $22.9°$ shows the excitation of the SPP wave.
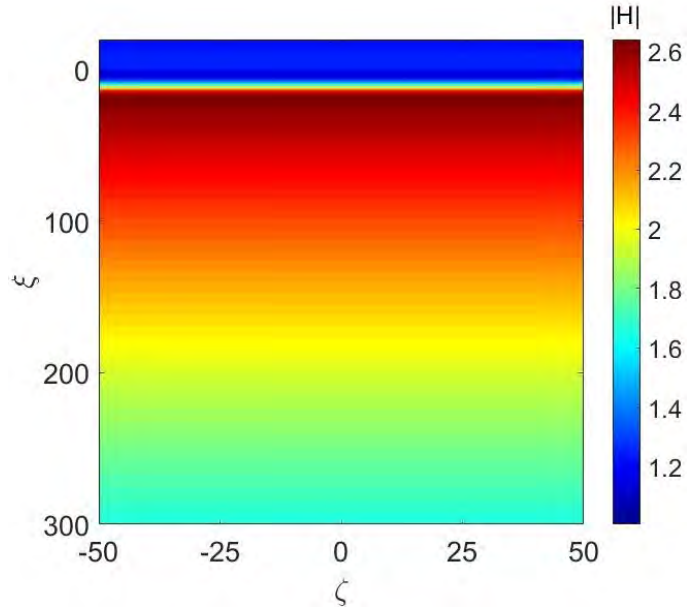
Figure 2.4: 2-D map depicting the variation of field intensity of SPP wave at $\theta_i = \theta_{SPP} = 22.9°$, where $n_1 = 2.6$, $n_2 = \sqrt{-54 + 21j}$ and $n_3 = 1$ and L=15 nm and $\lambda = 633$ nm.
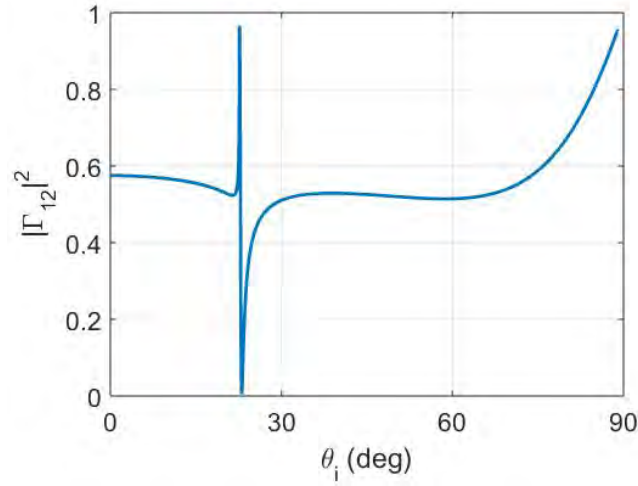
(a) $n_2 = \sqrt{-54 + 21j}$, $\lambda = 800$ nm, $\theta_{ssp} = 23.07°$
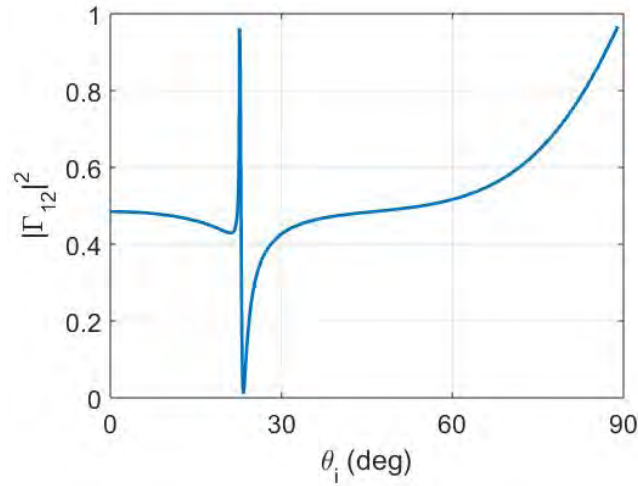
(b) $n_2 = \sqrt{-34 + 13j}$, $\lambda = 700$ nm, $\theta_{ssp} = 23.35°$

Figure 2.5: Reflectance is plotted as a function of the incident angle for different wavelengths and refractive indexes. The simulation parameters are $n_1 = 2.6$, $n_3 = 1$ and L=15 nm.
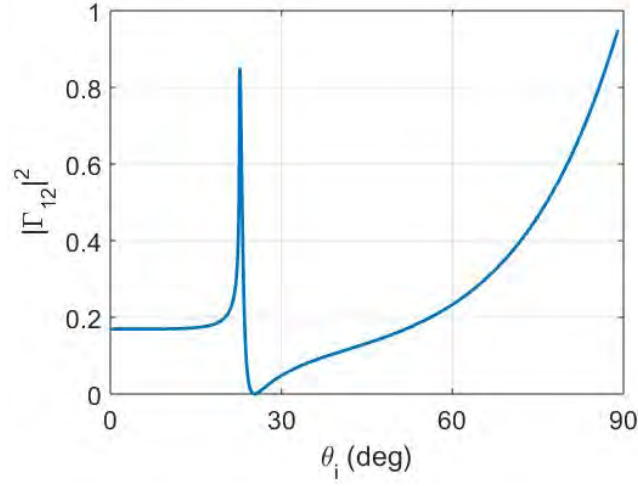
(a) $n_2 = \sqrt{-10 + 13j}$, $\lambda = 500$ nm, $\theta_{ssp} = 25.5°$
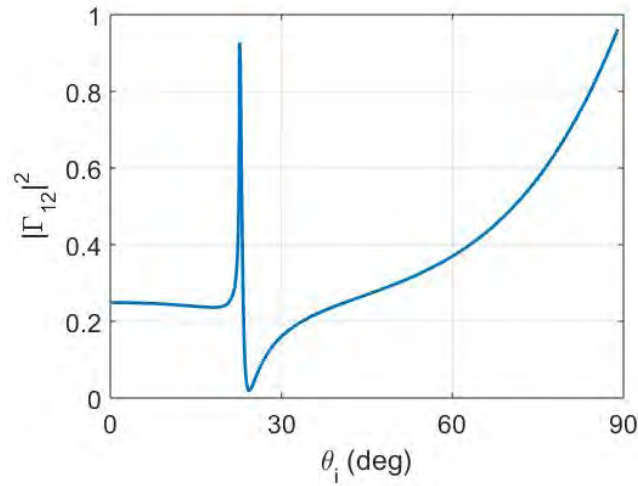
(b) $n_2 = \sqrt{-17 + 12j}$, $\lambda = 633$ nm, $\theta_{ssp} = 24.2°$

Figure 2.6: Reflectance as a function of incident angle. The parameters used are $n_1 = 2.6$, $n_3 = 1$, and L=15 nm.

2.3   Grating-coupled configuration

Grating-coupled configuration is another alternative to the TKR configuration, as shown in figure (2.7). Grating-coupled configuration is usually used to excite SPP waves. However, the configuration can also excite Tamm and Dyakonov-Tamm waves. To excite SPP waves, it is essential to illuminate periodic corrugations of metal. Moreover, the fields of partnering materials should be represented as Floquet harmonics. In case that the component of wave vector Floquet harmonics is identical to the SPP wave component, Floquet harmonics can be coupled with SPP waves. Note that the grating-coupled configuration also permits the inverse process of coupling a non-radiating SPP wave with light [156, 157]. This option offers a significant advantage over the TKR configuration as it offers better integration with the chemical sensor (SPP based) [158] into integrated circuits [159]. The grating-coupled configuration is also beneficial if it is needed to excite multiple SPP waves at the same time through a finite light source.
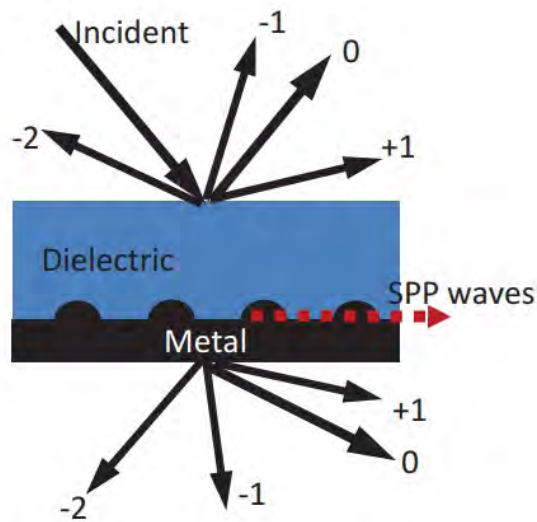
Figure 2.7: Grating-coupled configuration

2.4 SPP waves excitation using sinusoidal grating coupled configuration

Now, to excite the SPP wave using a sinusoidal grating, the geometry of the problem is depicted in figure (2.8). The parameters used in the figure are described in Table 2.1. A linearly polarized plane wave is incident on region 0 and its expression is given by
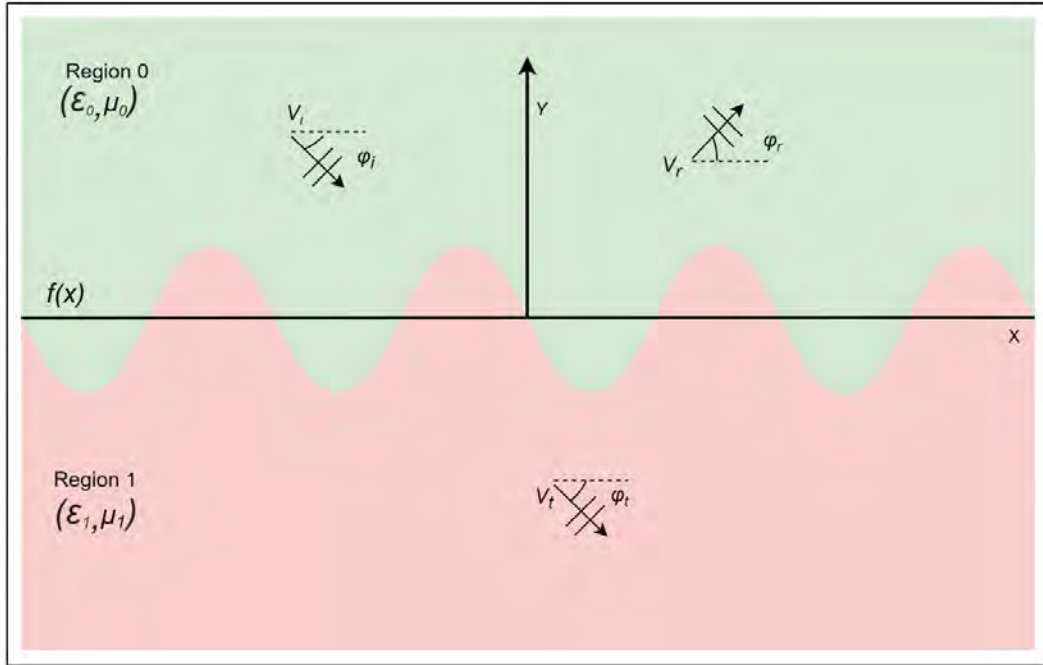
Figure 2.8: Geometry of the sinusoidal grating coupled approach to excite the SPP waves

$$V_i = V_0 e^{j(k_x^i x - k_{0y}^i y)} \qquad (2.15)$$

By Huygens principle and Green's identity, the total fields for region 0 are given by [73].

$$V_i(r) - \int_p d\sigma' \{G_{0p}(r,r')\hat{n}.\nabla'V_0(r') - V_0(r')\hat{n}.\nabla'G_{0p}(r,r')\} = V_0(r), \; y > f(x) \qquad (2.16)$$

Table 2.1: Description of parameters used in the geometry

Parameters	Descriptions
ϵ_0, μ_0	Permittivity and permeability of free space
ϵ_1, μ_1	Permittivity and permeability of region 1
$\varphi_i, \varphi_r, \varphi_t$	Angle of incidence, reflection and transmission, respectively
f(x)	grating profile
P_s	Period of the grating
h	Root mean square height grating

Use of the extinction theorem gives

$$V_i(r) - \int_p d\sigma' \{G_{0p}(r,r')\hat{n}.\nabla'V_0(r') - V_0(r')\hat{n}.\nabla'G_{0p}(r,r')\} = 0, \ y < f(x)$$
(2.17)

for region 1

$$\int_p d\sigma' \{G_{1p}(r,r')\hat{n}.\nabla'V_1(r') - V_1(r')\hat{n}.\nabla'G_{1p}(r,r')\} = \begin{cases} V_1(r) & y < f(x) \\ 0 & y > f(x) \end{cases}$$
(2.18)

where $G_{tP_s}(r,r')$ is periodic Green's function defined as

$$G_{tP_s}(r,r') = -\frac{1}{2jP_s}\sum_n \frac{1}{k_{tyn}}\exp(jk_{xn}(x-x') + jk_{tyn}\mid y-y'\mid) \quad (2.19)$$

In the above equation, $k_{xn} = k_x^i + \frac{2n\pi}{P_s}$ and $k_{tyn} = \sqrt{k_t^2 - k_{xn}^2}$. Substituting the value of Green functions in equations (2.16), (2.17) and (2.18), we get

$$V_0(r) = V_i(r) + \sum_{n=-\infty}^{\infty} \gamma_{01n}\frac{e^{j(k_{0nx}x + k_{0ny}y)}}{\sqrt{k_{0ny}}} \quad y > f_{(max)} \quad (2.20)$$

$$0 = V_i(r) - \sum_{n=-\infty}^{\infty} a_{0n}\frac{e^{j(k_{0nx}x - k_{0ny}y)}}{\sqrt{k_{0ny}}} \quad y < f_{(max)} \quad (2.21)$$

and

$$V_1(r) = \sum_{n=-\infty}^{\infty} \tau_{01n} \frac{e^{j(k_{1nx}x - k_{1ny}y)}}{\sqrt{k_{1ny}}} \quad y > f_{(max)} \tag{2.22}$$

$$0 = -\sum_{n=-\infty}^{\infty} a_{1n} \frac{e^{j(k_{1nx}x + k_{1ny}y)}}{\sqrt{k_{1ny}}} \quad y < f_{(max)} \tag{2.23}$$

where

$$\gamma_{01n} = \frac{1}{2jkP_s} \int_{P_s} d\sigma' \left\{ \frac{e^{-jk_{0n}^+ r(x')}}{\sqrt{k_{0n}}} \hat{n}'.\nabla' V_0(r') - V_0(r')\hat{n}'.\nabla' \frac{e^{-jk_{0n}^+ r(x')}}{\sqrt{k_{0n}}} \right\} \tag{2.24}$$

$$\tau_{01n} = \frac{-1}{2jk_1 P_s} \int_{Ps} d\sigma' \left\{ \frac{e^{-jk_{1n}^- r(x')}}{\sqrt{k_{1n}}} \hat{n}'.\nabla' V_1(r') - V_1(r')\hat{n}'.\nabla' \frac{e^{-jk_{1n}^- r(x')}}{\sqrt{k_{1n}}} \right\} \tag{2.25}$$

$$a_{0n} = \frac{-1}{2jkP_s} \int_{Ps} d\sigma' \left\{ \frac{e^{-jk_{0n}^- r(x')}}{\sqrt{k_{0n}}} \hat{n}'.\nabla' V_0(r') - V_0(r')\hat{n}'.\nabla' \frac{e^{-jk_{0n}^- r(x')}}{\sqrt{k_{0n}}} \right\} \tag{2.26}$$

$$a_{1n} = \frac{1}{2jk_1 P_s} \int_{Ps} d\sigma' \left\{ \frac{e^{-jk_{1n}^+ r(x')}}{\sqrt{k_{1n}}} \hat{n}'.\nabla' V_1(r') - V_1(r')\hat{n}'.\nabla' \frac{e^{-jk_{1n}^+ r(x')}}{\sqrt{k_{1n}}} \right\} \tag{2.27}$$

The boundary conditions can be written in terms of unit vector normal to the surface $\hat{n}$ and they are given by

$$V_0 = V_1 \tag{2.28}$$

$$\hat{n}.\nabla' V_0 = \hat{n}.\nabla' V_1 \tag{2.29}$$

Expansion of the surface fields is used in EBCM. Here we use the following Fourier series expansion [160]

$$V_1 = \sum_n 2w_n \exp(ik_{xn}x) \tag{2.30}$$

$$d\sigma \hat{n}.\nabla' V_1 = jk_1 dx \sum_n 2q_n \exp(jk_{xn}x) \tag{2.31}$$

where w_n and q_n are unknown coefficients. Putting the fields V_1 and $\hat{n}.\nabla' V_1$ in boundary conditions and after some algebra, the following matrix equations

are obtained

$$
\begin{bmatrix} a \\ 0 \end{bmatrix} = \begin{bmatrix} S_N^- & c_2 \frac{k_1}{k} R_D^- \\ S_{N1}^+ & R_{D_1}^+ \end{bmatrix} \begin{bmatrix} w \\ q \end{bmatrix} \tag{2.32}
$$

$$
\begin{bmatrix} \gamma_{01} \\ \tau_{01} \end{bmatrix} = \begin{bmatrix} -S_N^+ & -c_2 \frac{k_1}{k} R_D^+ \\ S_{N1}^- & R_{D_1}^- \end{bmatrix} \begin{bmatrix} w \\ q \end{bmatrix} \tag{2.33}
$$

being

$$
\left[R_D^\pm \right]_{mn} = \pm \frac{1}{P_s} \int_{P_s} dx \, \frac{e^{-jk_m{}^\pm \rho(x)}}{\sqrt{k_{0ym}}} \exp(jk_{xn}x) \tag{2.34}
$$

$$
\left[S_N^\pm \right]_{mn} = \pm \frac{1}{jP_s} \int_{P_s} \left\{ d\sigma . \nabla \frac{e^{-jk_m{}^\pm \rho(x)}}{\sqrt{k_{0ym}}} \right\} \exp(jk_{xn}x) \tag{2.35}
$$

$$
\left[R_{D1}^\pm \right]_{mn} = \pm \frac{1}{P_s} \int_{P_s} dx \, \frac{e^{-jk_{1m}{}^\pm \rho(x)}}{\sqrt{k_{1ym}}} \exp(jk_{xn}x) \tag{2.36}
$$

$$
\left[S_{N1}^\pm \right]_{mn} = \pm \frac{1}{jP_s} \int_{P_s} \left\{ d\sigma . \nabla \frac{e^{-jk_{1m}^\pm \rho(x)}}{\sqrt{k_{1ym}}} \right\} \exp(jk_{xn}x) \tag{2.37}
$$

and

$$
c_2 = \begin{cases} \frac{\epsilon_1}{\epsilon_0} \frac{k^2}{k_1^2} & \text{TM case} \\ \frac{\epsilon_0}{\epsilon_1} \frac{k_1^2}{k^2} & \text{TE case} \end{cases} \tag{2.38}
$$

for a sinusoidal grating/surface, $f(x) = -h \cos(2\pi/P_s x)$ the elements of matrices are given by

$$
\left[R_D^\pm \right]_{mn} = \frac{-1}{\sqrt{k_{0ym}}} (\pm j)^{|m-n|} J_{|m-n|}(k_{0ym}h) \tag{2.39}
$$

$$
\left[S_N^\pm \right]_{mn} = \frac{-k_o^2 + k_{0xm}k_{0xn}}{\pm k_{0ym}} \left[R_D^\pm \right]_{mn} \tag{2.40}
$$

$$\left[R_{D_1}^{\pm}\right]_{mn} \quad = \quad \frac{-1}{\sqrt{k_{1ym}}}(\pm j)^{|m-n|}J_{|m-n|}(k_{1ym}h) \tag{2.41}$$

$$\left[S_{N1}^{\pm}\right]_{mn} \quad = \quad \frac{-k_1^2 + k_{1xm}k_{1xn}}{\pm k_{1ym}}\left[R_{D_1}^{\pm}\right]_{mn} \tag{2.42}$$

2.4.1 Results and discussion

To verify the numerical implementation, diffraction efficiency $|\gamma_{01(-1)}|^2$ of order -1 and total power $|\gamma_{01n}|^2$ are evaluated in figure (2.9) [72]. The parameters used to obtain the results are period P_s = 1205 nm, height of the surface h = 100 nm, and wavelength $\lambda = 476$ nm. The sinusoidal profile is coated with silver having permittivity $\epsilon_1 = (-7.0410 + 0.2781j)\epsilon_0$. The dips in the total reflected efficiencies shows the excitation of SPP waves. The SPP waves are excited at angles $-18.5°$, $18.5°$, and $45.8°$.

The dispersion relation for the grating is given [72]

$$\sin(\theta_i) + n\frac{\lambda}{P_s} = \sqrt{\frac{\epsilon_1'}{\epsilon_1' + \epsilon_0}} \tag{2.43}$$

In the equation (2.43), where n is an integer. This equation is an approximation and does not account for the surface height. The angles, $16.8°$ and $43.19°$, are determined using the aforementioned formula at which SPP waves excite. These angles closely align with those depicted in the figure (2.9).

The excitation angle can be shifted by varying the material's wavelength and permittivity. It can be noticed in figure (2.10b) that the excitation angles shifted to $-30.8°$ and $30.8°$ where wavelength $\lambda = 647$ nm and its corresponding permittivity is $\epsilon_1 = (-17.4091 + 0.5792j)\epsilon_0$ by Drude model. The curves corresponding to positive and negative orders exhibit a high degree of similarity, differing only in the reversal of the sign of the angle of incidence.

Now we consider the sinusoidal profile coated with aluminum having permittivity $\epsilon_1 = (-20.5703 + 5.096j)\epsilon_0$, at $\lambda = 476$ nm. The simulation results are given in figure (2.11b). The SSP waves excite at angles $-14.8°$, $14.8°$ and $40.4°$. These angles are changed to $-37.1°$, $-10°$, $9.8°$ and $37.1°$ when $\lambda = 521$ nm with $\epsilon_1 = (-24.7236 + 6.8130j)\epsilon_0$ as depicted in figure (2.12b).

Finally, a profile coated with gold characterized with permittivities $\epsilon_1 = (-11.9914 + 1.3346j)\epsilon_0$ at $\lambda = 476$ nm is assumed in figure (2.13). The SPP waves are excited at different angles than those observed for silver and aluminum. Figure (2.14) shows the result for $\lambda = 568$ nm with $\epsilon_1 = (-6.5972 + 1.5537j)\epsilon_0$. The angles of excitation are significantly changed.

(a)

(b)
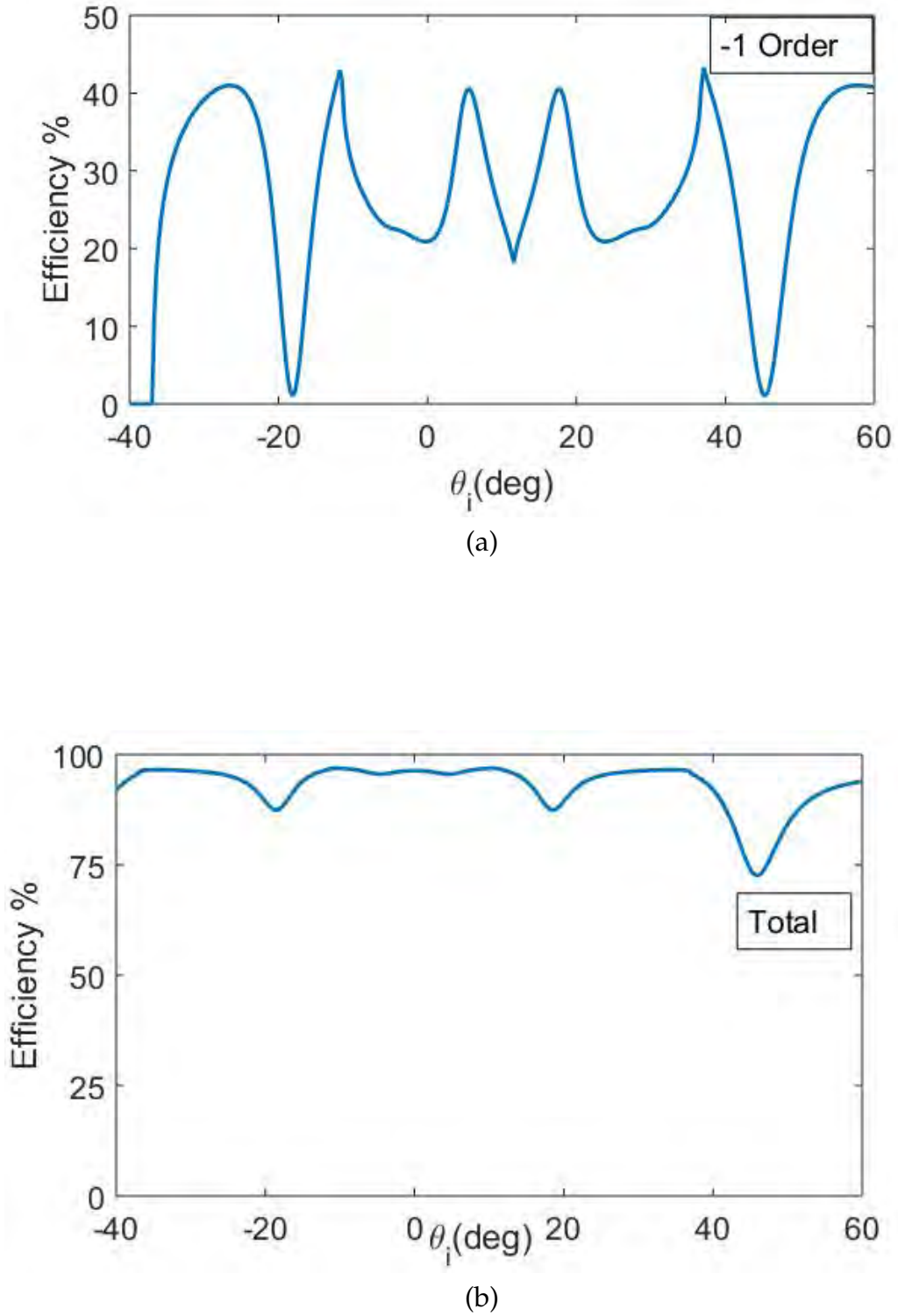
Figure 2.9: (a) The diffraction efficiency $|\gamma_{01(-1)}|^2$ of order -1, and (b) total power $|\gamma_{01n}|^2$. The profile is coated with silver while the simulation parameters are λ=476 nm, P_s=1205 nm, h= 100 nm, and $\epsilon_1 = (-7.0410 + 0.2781j)\epsilon_0$.

(a)

(b)
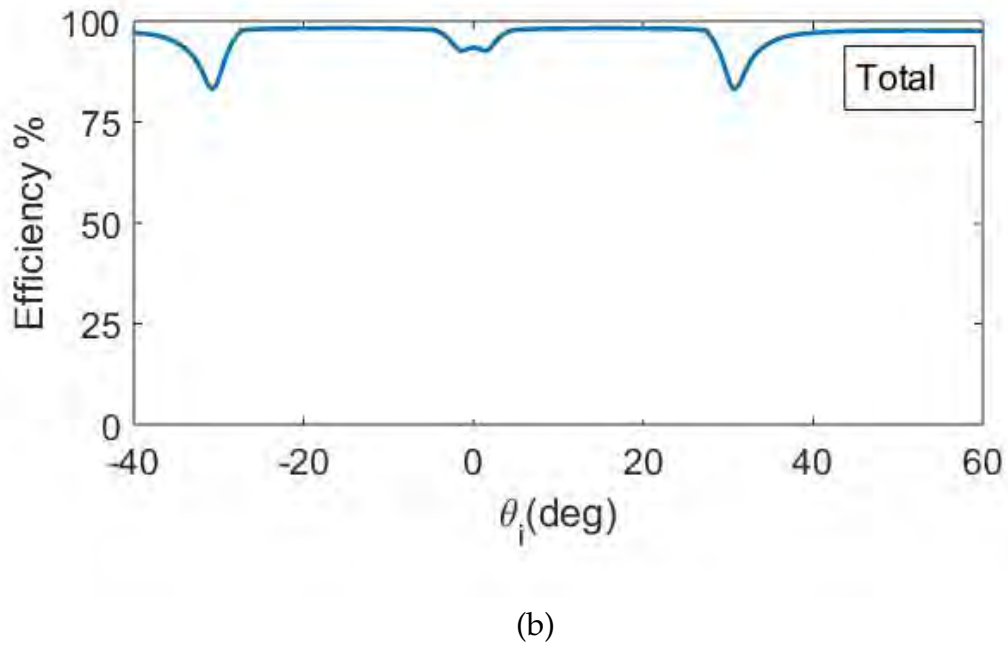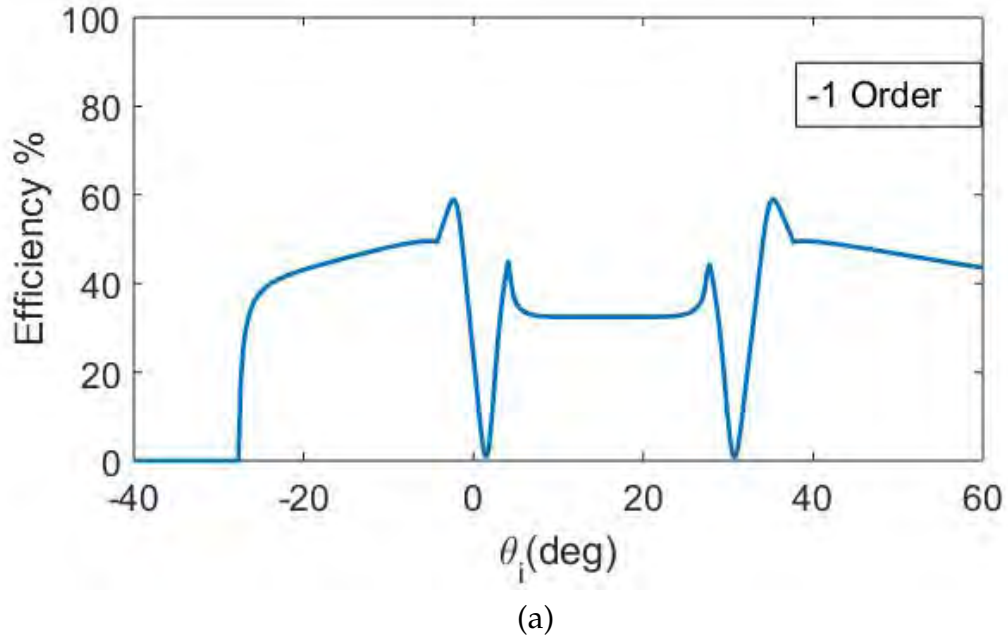
Figure 2.10: (a) The diffraction efficiency $|\gamma_{01(-1)}|^2$ of order -1, and (b) total power $|\gamma_{01n}|^2$ are plotted as a function of incident angle. The profile is coated with silver while the simulation parameters are λ=647 nm, P_s=1205 nm, h= 100 nm, and $\epsilon_1 = (-17.4091 + 0.5792j)\epsilon_0$.

31

(a)

(b)
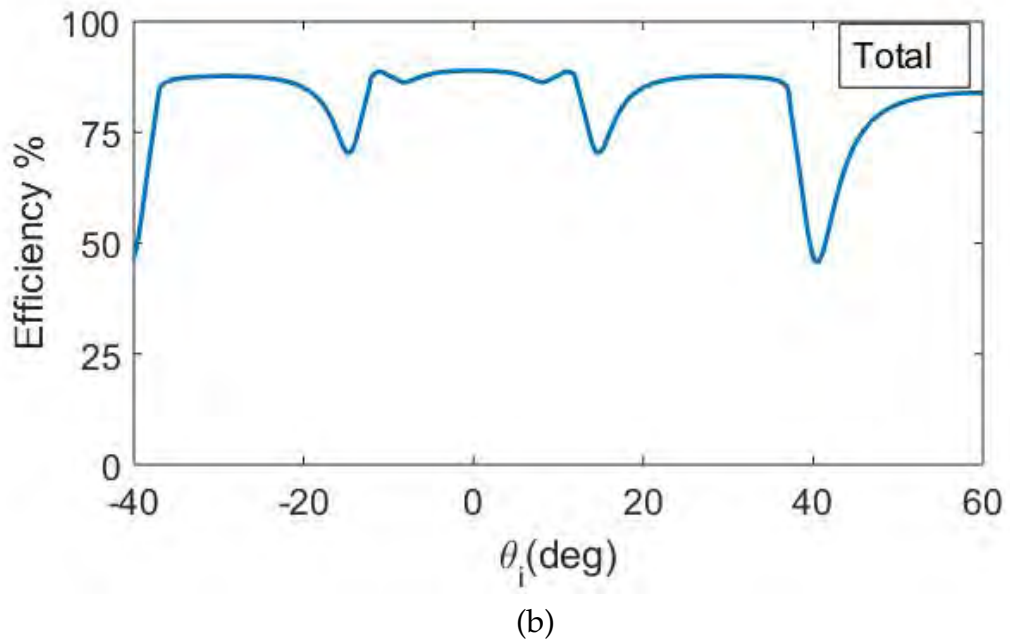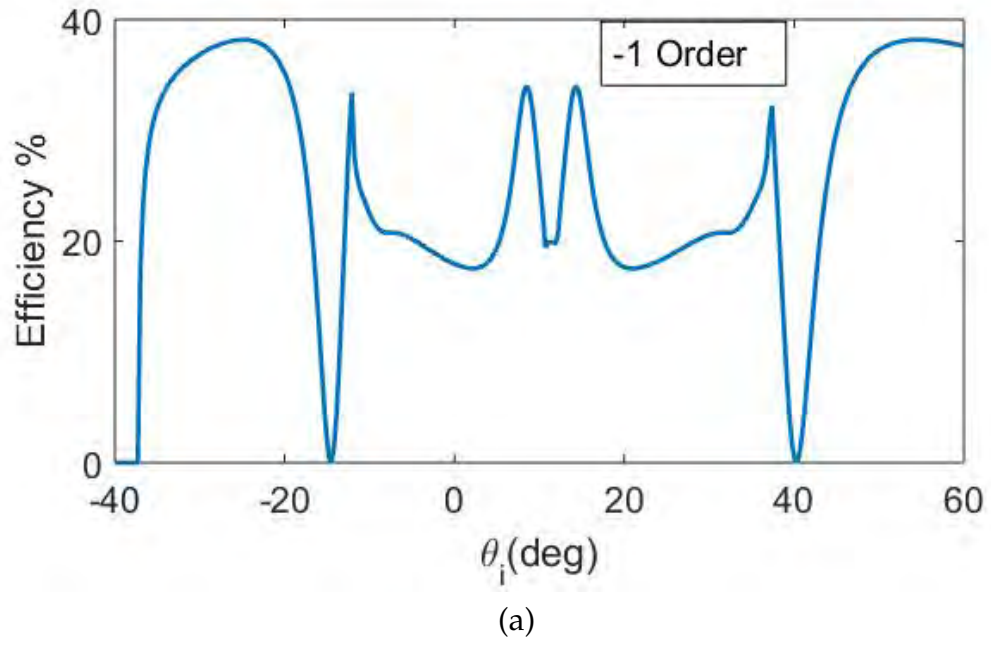
Figure 2.11: Results for a profile coated with aluminum for $\epsilon_1 = (-20.5703 + 5.096j)\epsilon_0$, λ=476 nm, P_s=1205 nm, h= 100 nm.

(a)

(b)
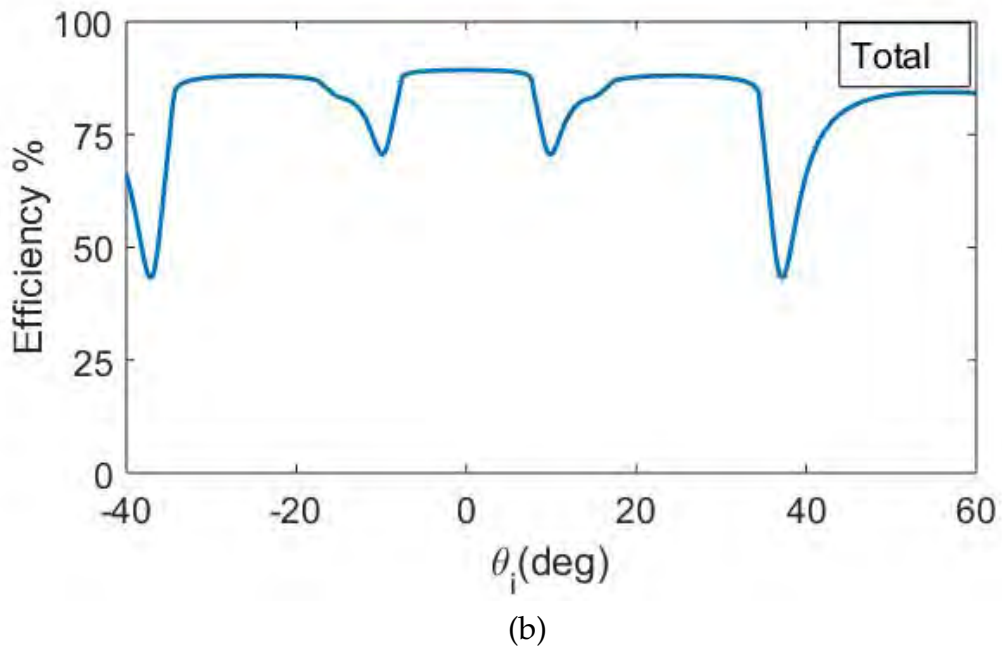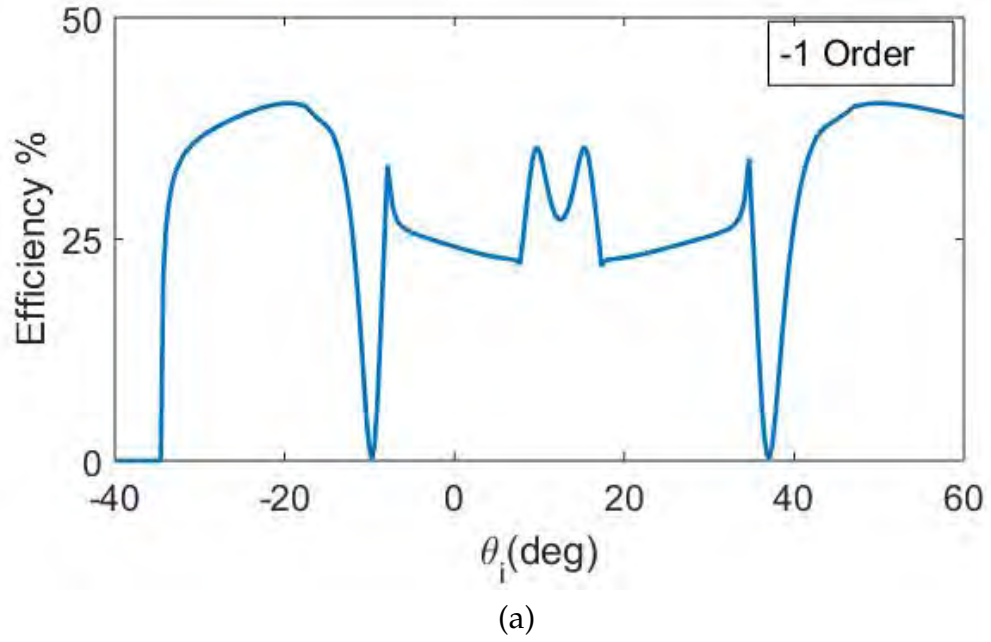
Figure 2.12: Same as figure 2.11 except $\epsilon_1 = (-24.7236 + 6.8130j)\epsilon_0$, $\lambda = 521$ nm.

(a)

(b)
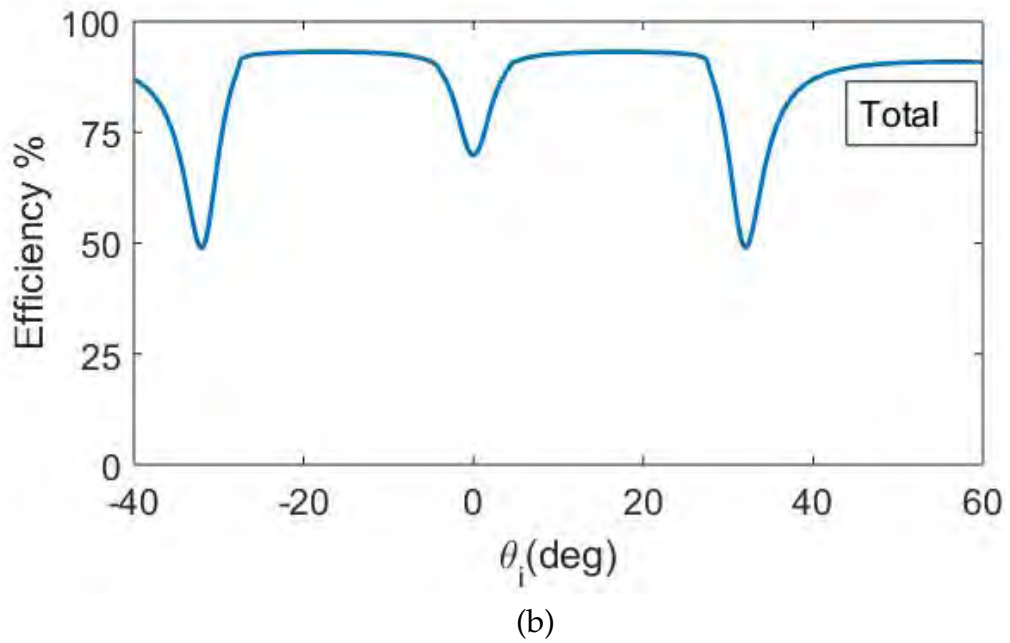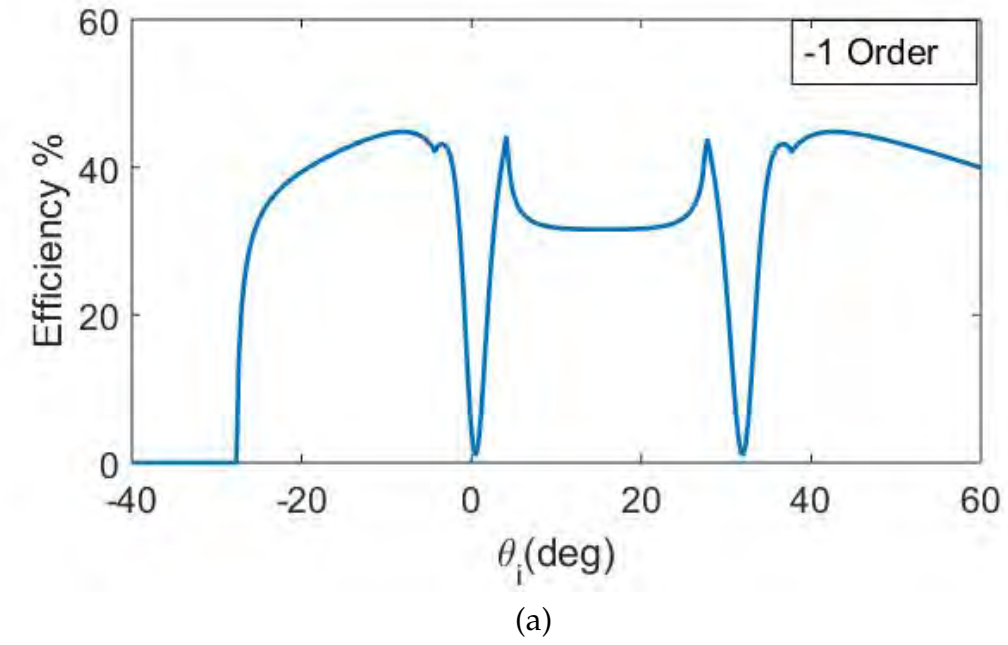
Figure 2.13: Diffraction efficiency for a profile coated with gold having $\epsilon_1 = (-11.9914 + 1.3346j)\epsilon_0$, $\lambda = 476$ nm, P_s=1205 nm and h= 100 nm.
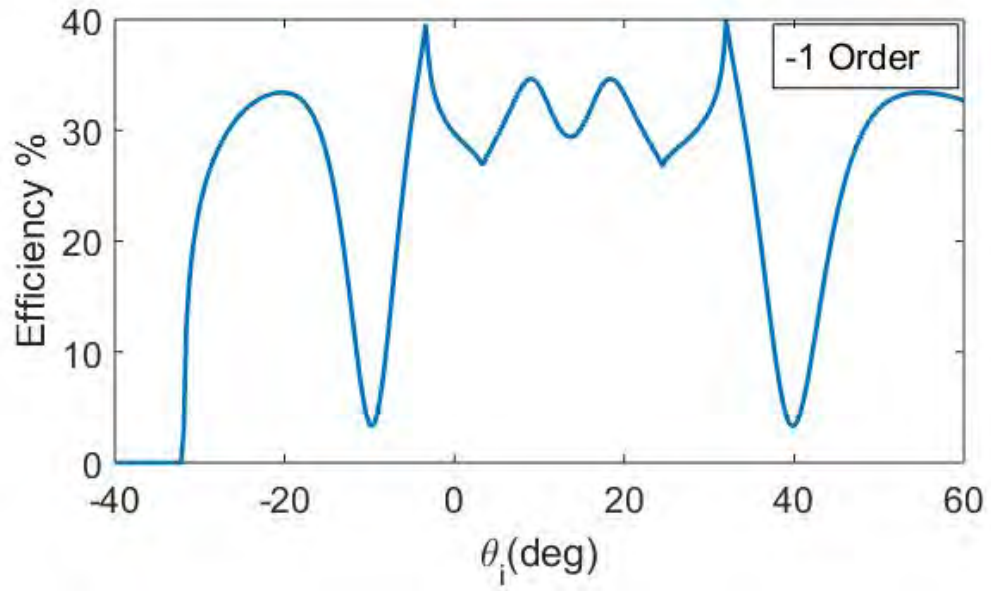
(a)
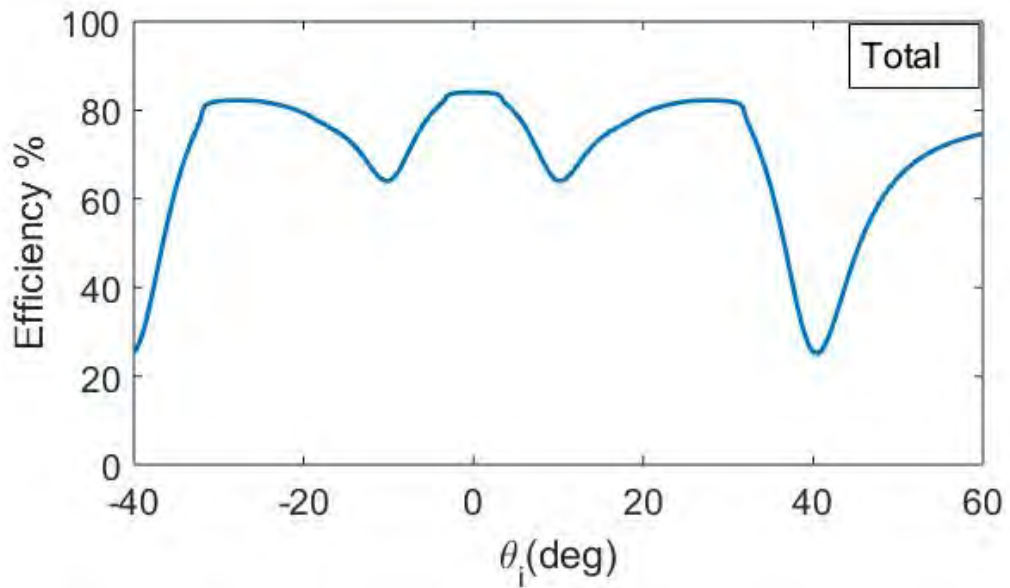
(b)

Figure 2.14: Same as figure 2.13 except $\epsilon_1 = (-6.5972 + 1.5537j)\epsilon_0$, $\lambda = 568$ nm.

Chapter 3

Enhanced scattering in the presence of SPP waves excited by TKR configuration

In this chapter, a formulation based on cylindrical wave approach has been applied to study the SPP wave scattering form different structures made from N metallic circular scatterers. A TKR configuration involving a dielectric/metallic interface is used to excite the SPP waves. The cylindrical wave functions are used as the basis function for the representation of scattered fields. The analytical formulation is reported in section (3.1) while numerical results are given in section (3.2).

3.1 Analytical formulation

The schematic to excite the SPP wave at $\xi = \Lambda$ is shown in figure (3.1). A configuration is made to excite the SSP wave similar to TKR [153, 154]. Medium 1 is considered a high refractive index medium to work as a prism to excite SPP waves, with permittivity of $\epsilon_1 = \epsilon_o \epsilon_{r1}$, while medium 2 is a metallic layer with permittivity of $\epsilon_2 = \epsilon_o \epsilon_{r2}$. The medium 3 has a permittivity of $\epsilon_3 = \epsilon_o$. Throughout the chapter, an $e^{-j\omega t}$ time convention is assumed and suppressed in the formulations, while all the media are considered non-magnetic, homoge-
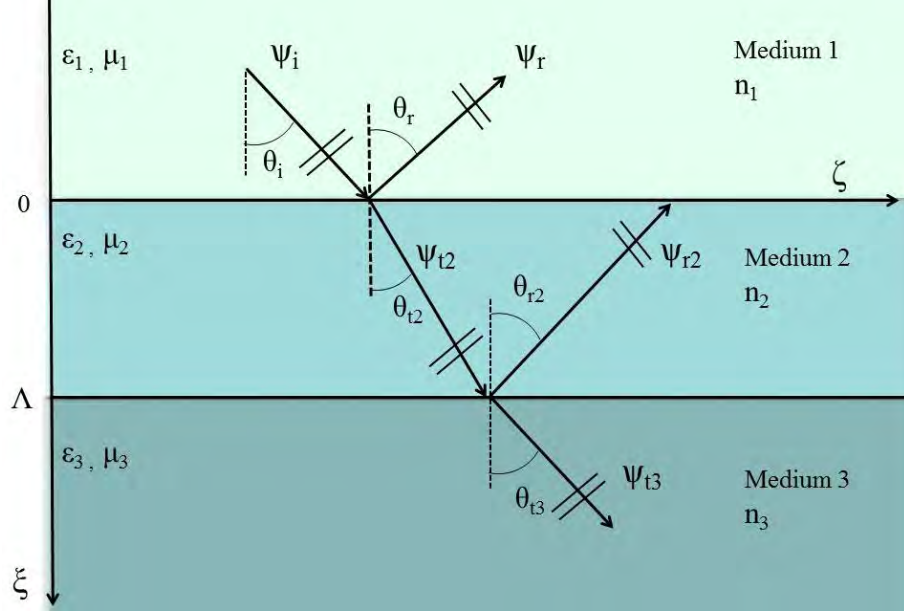
Figure 3.1: Schematic to the excite SPP wave at interface $\xi = \Lambda$, where normalized co-ordinates $\xi = k_1 x$ and $\zeta = k_1 z$ are utilized.

nous, linear, and isotropic. The field components are defined in Table 3.1. To find the angle of excitation of the SPP wave, first reflection and transmission coefficients are found for plane wave incident upon the interface at $\xi = 0$. The coefficients such as $\Gamma_{12}(n_\parallel^i)$, $T_{12}(n_\parallel^i)$, $\Gamma_{23}(n_\parallel^i)$ and $T_{23}(n_\parallel^i)$ are described in Table 3.2 and their expressions can be found in [155].

Table 3.1: The involved fields in each medium to excitation of SPP waves.

Field components	Descriptions
$\psi_i(\xi, \zeta)$	Incident plane wave at $\xi < 0$
$\psi_r(\xi, \zeta)$	Reflected plane wave at $\xi < 0$
$\psi_{t2}(\xi, \zeta)$	Transmitted plane wave at $0 < \xi < \Lambda$
$\psi_{r2}(\xi, \zeta)$	Reflected plane wave at $0 < \xi < \Lambda$
$\psi_{t3}(\xi, \zeta)$	Transmitted plane wave at $\xi > \Lambda$

Now we consider the schematic shown in figure (3.2) to study the effect of SPP waves on scattering from a corner reflector and a strip. Figure (3.3)

Table 3.2: Reflection and transmission coefficients to calculate reflectance/transmittance and angle of SPP wave excitation.

Coefficients	Descriptions
Γ_{12}	Reflection coefficient for the interface between medium 1 and medium 2.
T_{12}	Transmission coefficient for the interface between medium 1 and medium 2.
Γ_{23}	Reflection coefficient for the interface between medium 2 and medium 3.
T_{23}	Transmission coefficient for the interface between medium 2 and medium 3.
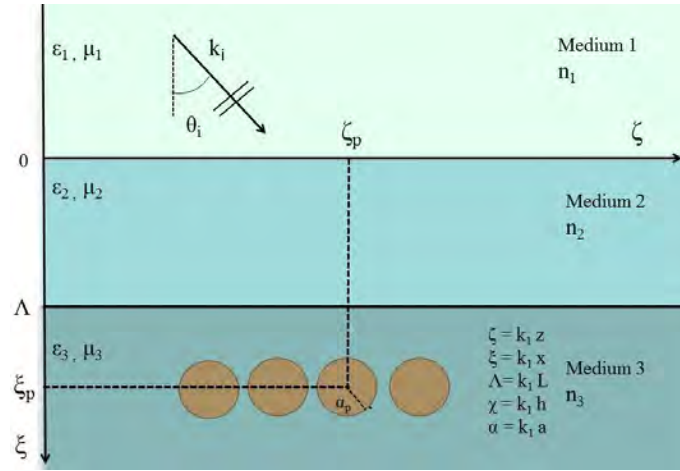
Figure 3.2: A scenario to study the SPP wave scattering from different cylindrical structures such as corner reflector, strip, etc, where the involved geometrical and physical parameters are reported inside the geometry.

depicts the arrangement of small metallic circular scatterers to simulate the structures. The same area rule is used to determine the size of small circular scatterers [161]. We assume the main reference frame (MRF) (O, ξ, ζ) described by normalized coordinates $\xi = k_1 x$, $\zeta = k_1 z$ and the reference frames RF_p centered on the axis of the p-th scatterer (p = 1, 2, ..., N). The other involved geometrical parameters are also described. According to cylindrical scattering problems, the convention for polarizations such as TE/TM is used when the electric/magnetic field is transverse to the axis of the scatterer as

$$\psi(\xi, \zeta) = E_y(\xi, \zeta), \quad \text{TM-Polarization}$$
$$\psi(\xi, \zeta) = H_y(\xi, \zeta), \quad \text{TE-Polarization}$$

The $\psi(\xi, \zeta)$ function represents the multiple field contributions in each medium
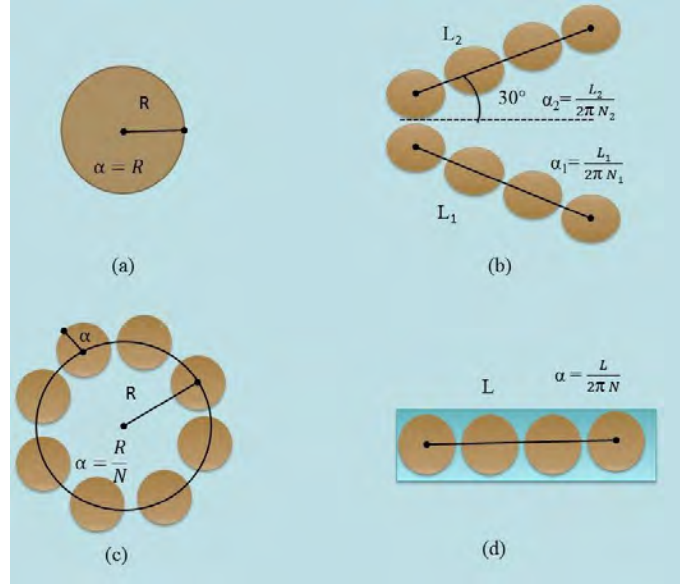
Figure 3.3: Simulation of different shapes by the arrangement of circular scatterers such as corner reflector, strip, etc, to observe the effect of SPP waves excitation on scattering.

due to the incident field. In Table 3.3 the field components are defined when the scatter is present. The transmitted field into medium 3 will incident on the object.

Table 3.3: Description of scattered field components in the presence of scatterers.

Field components	Descriptions
$\psi_{st}^1(\xi,\zeta)$	Scattered transmitted field through the interface at $\xi = 0$
$\psi_{sr}^2(\xi,\zeta)$	Scattered reflected field from the interface at $\xi = 0$
$\psi_{st}^2(\xi,\zeta)$	Scattered transmitted field through the interface at $\xi = \Lambda$
$\psi_s(\xi,\zeta)$	Scattered field from the cylindrical objects
$\psi_{sr}(\xi,\zeta)$	Scattered reflected field from the interface at $\xi = \Lambda$

In order to take into account the circular geometry of scatterers, the transmitted field (2.5) will be transformed into the polar coordinate system centered on the

p_{th} scatterer can be written as [161]

$$\psi_{t3}(\xi,\zeta) = \psi_0 T_{12}(n_\parallel^i) T_{23}(n_\parallel^i) e^{jn_3(n_\perp^{t3}(\chi_p-\Lambda)+n_\parallel^{t3}\eta_p)} \sum_{\ell=-\infty}^{\infty} j^\ell J_\ell(n_3\rho) e^{j\ell\theta_p} e^{j\ell\theta_{t3}} \quad (3.1)$$

where $n_\perp^{t3}$ and $n_\parallel^{t3}$ are the orthogonal and parallel components of the wave vector [161]. Resulting of the incident field, the scattered field may be written as

$$\psi_s(\xi,\zeta) = \psi_0 \sum_{q=1}^{N} \sum_{m=-\infty}^{\infty} c_{qm} CW_m(n_3\xi_q, n_3\zeta_q), \quad \xi > \Lambda \quad (3.2)$$

where $CW_m(\xi_q,\zeta_q) = H_m^{(1)}(\rho_q) e^{jm\theta_q}$ is a cylindrical function in terms of the first kind of Hankel function of order m. The plane wave spectrum of CW_m is

$$CW_m(n_3\xi_q, n_3\zeta_q) = \frac{1}{2\pi} \int_{-\infty}^{\infty} F_m(\xi, n_\parallel) e^{jn_\parallel\zeta_q} dn_\parallel \quad (3.3)$$

where Fourier spectrum is:

$$F_m(\xi, n_\parallel) = \frac{2e^{j|\zeta|}\sqrt{1-n_\parallel^2}}{1-n_\parallel^2} \begin{cases} e^{-jm\arccos n_\parallel}, & \xi \le 0, \\ e^{jm\arccos n_\parallel}, & \xi \ge \Lambda, \end{cases} \quad (3.4)$$

with the use of the addition theorem of Hankel function equation (3.2) may be written as [161]

$$\psi_s(\xi,\zeta) = \psi_0 \sum_{\ell=-\infty}^{\infty} J_\ell(n_3\rho_p) e^{j\ell\theta_p} \sum_{q=1}^{N} \sum_{m=-\infty}^{\infty} c_{qm}$$

$$\times \left[CW_{m-\ell}(n_3\xi_{qp}, n_3\zeta_{qp})(1-\delta_{qp}) + \frac{H_\ell^{(1)}(n_3\rho_p)}{J_\ell(n_3\rho_p)} \delta_{qp}\delta_{\ell m} \right] \quad (3.5)$$

Expressing the scattered reflected field at the secondary reference frame cen-

tered on the q_{th} scatterer is given as

$$
\psi_{sr}(\xi_q, \zeta_q) = \psi_0 \sum_{\ell=-\infty}^{\infty} J_\ell(n_3\rho_p)e^{j\ell\theta_p} \sum_{q=1}^{N} \sum_{m=-\infty}^{\infty} c_{qm}
$$
$$
\times RW_{m+\ell}[-n_3(\chi_q + \chi_p - 2\Lambda), n_3(\eta_q - \eta_p)], \quad \xi > \Lambda \tag{3.6}
$$

where

$$
RW_m(\xi, \zeta) = \frac{1}{2\pi} \int_{-\infty}^{\infty} \Gamma_{32}(n_\parallel)F_m[n_3(\xi - \Lambda), n_\parallel]e^{jn_2 n_\parallel \zeta}dn_\parallel \tag{3.7}
$$

We observe the scattered field that is transmitted through the interface at $\xi = 0$ and it is described as

$$
\psi_{st}^1(\xi, \zeta) = \psi_0 \sum_{q=1}^{N} \sum_{m=-\infty}^{\infty} c_{qm} TW_m^1(\xi, \zeta; \chi_q), \quad \xi < 0, \tag{3.8}
$$

where

$$
TW_m^1(\xi_p, \zeta_p; \chi_p) = \frac{1}{2\pi} \int_{-\infty}^{\infty} T_{21}(n_\parallel)T_{32}(n_\parallel)F_m[-n_3(\chi_q - \Lambda), n_\parallel]
$$
$$
\times e^{-j\sqrt{1-\left(n_3 n_\parallel\right)^2}\xi} e^{jn_3 n_\parallel(\zeta - \eta_q)}dn_\parallel \tag{3.9}
$$

Applying the boundary condition at $\rho_p = k_1\alpha_p$ on the surface of the scatterer for both polarizations we get

$$
\begin{aligned}
\psi_{t3} + \psi_s + \psi_{sr} \mid_{\rho_p = k_1\alpha_p} &= 0 \quad \text{TM - polarization} \\
\frac{\partial}{\partial \rho_p}(\psi_{t3} + \psi_s + \psi_{sr}) \mid_{\rho_p = k_1\alpha_p} &= 0 \quad \text{TE - polarization}
\end{aligned} \tag{3.10}
$$

By putting equations (3.1), (3.2) and (3.6) in equation (3.10) and rearranging we get [161]

$$
\sum_{q=1}^{N} \sum_{m=-\infty}^{\infty} A_{m\ell}^{qp(TM,TE)} c_{qm} = B_\ell^{p(TM,TE)}, \quad
\begin{cases}
\ell = 0, \pm 1, \pm 2 ..... \pm \infty \\
p = 1, ...N
\end{cases} \tag{3.11}
$$

where

$$
A_{m\ell}^{qp(TM,TE)} = j^{-\ell} G_\ell^{(TM,TE)} \times
$$

$$
\left\{ CW_{m-\ell}(n_3\xi_{qp}, n_3\zeta_{qp})(1 - \delta_{qp}) + \frac{\delta_{qp}\delta_{\ell m}}{G_\ell^{(TM,TE)}(n_3\rho_p)} \right.
$$

$$
\left. + RW_{m+\ell}\left[-n_3(\chi_p + \chi_p - 2\Lambda), n_3(\eta_p - \eta_q)\right] \right\} \tag{3.12}
$$

and

$$
B_\ell^{p(TM,TE)} = -G_\ell^{(TM,TE)} \left\{ T_{21}(n_\parallel^i) T_{32}(n_\parallel^i) e^{jn_3\left[n_\perp^{t3}(\chi_p - \Lambda) + n_\parallel^{t3}\eta_p\right]} e^{-j\ell\theta_{t3}} \right\} \tag{3.13}
$$

while δ_{qp} and δ_{lm} are Kronecker delta functions and

$$
G_\ell^{(TM)} = \frac{J_\ell(x)}{H_\ell^{(1)}(x)} \tag{3.14}
$$

$$
G_\ell^{(TE)} = \frac{J_\ell'(x)}{H_\ell'^{(1)}(x)} \tag{3.15}
$$

3.2   Numerical results

The linear system in equation (3.11) is numerically solved by taking the truncation index to $M = 3n_2a$ [161]. The scattering properties are studied by excitation of the SPP waves using the Turbadar–Kretschmann–Raether (TKR) configuration. The refractive index of the prism is $n_1 = 2.6$ and the operating wavelength is 633 nm. We have assumed an aluminum and air interface with $n_2 = \sqrt{-54 + 21j}$, $n_3 = 1$ at L= 15 nm, respectively, along which the SPP wave propagates. Moreover, the excitation angle is $\theta_i = \theta_{SPP} = 22.9°$ can be found by computing the reflectance as a function of incidence angle θ_i. In the subsequent discussion, we have considered multiple structures such as corner reflector, strip, etc., simulated by circular scatterers and observed the scattering properties. First, we validate the implementation by reproducing the figure (3.4) in the presence and absence of the SPP waves. The reader is referred to

figures (6) and (7) of [54] for more details. The simulation parameters remain the same in further simulations.

(a) R = 10 nm, $\theta_i = \theta_{\text{SPP}} = 22.9°$

(b) R = 10 nm, $\theta_i = 12.9°$

(c) h = 100 nm, $\theta_i = \theta_{\text{SPP}} = 22.9°$

(d) h = 100 nm, $\theta_i = 12.9°$
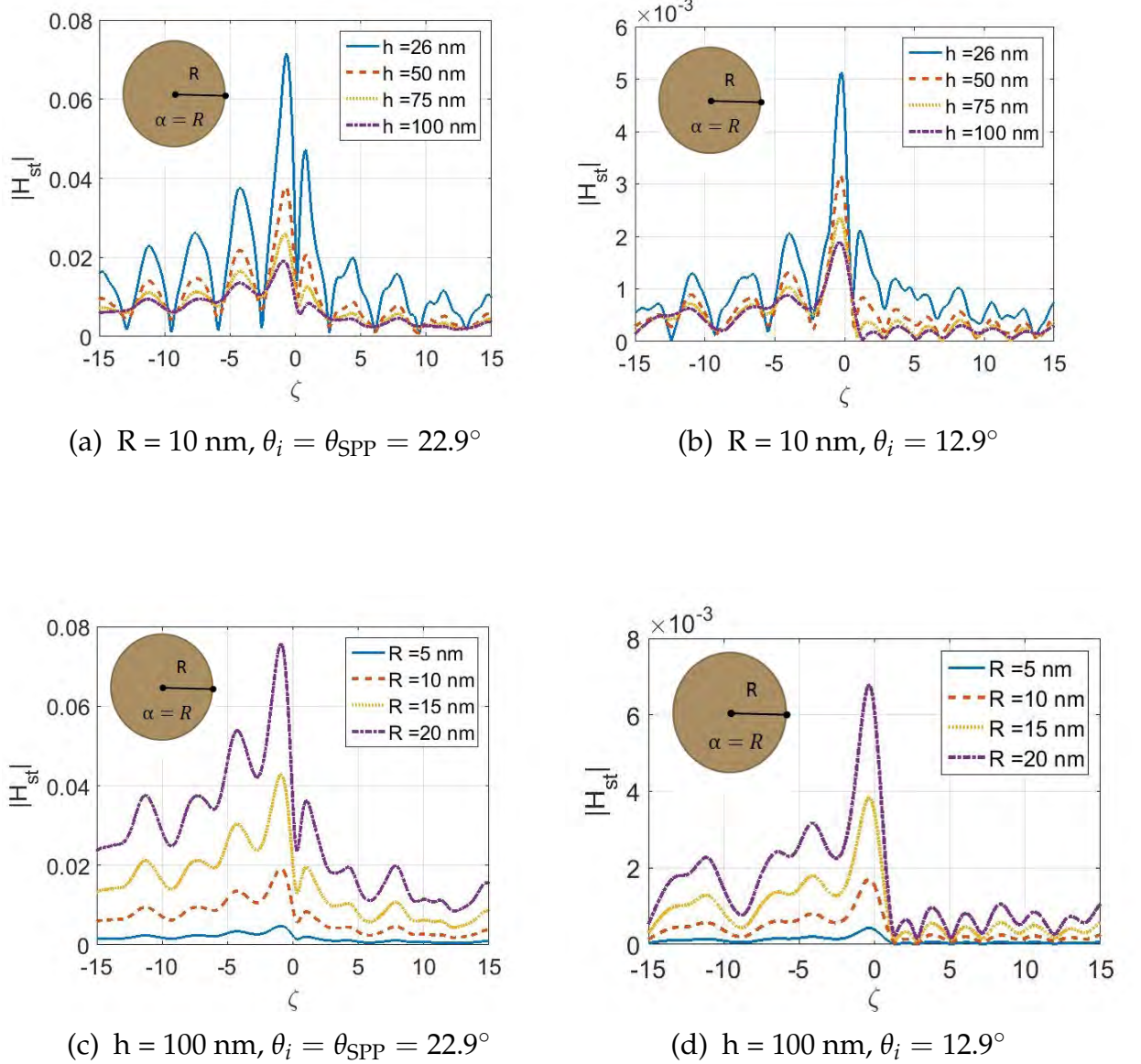
Figure 3.4: Effect of SPP waves on the scattered field for a single scatterer. Comparison is done with the scattered field in the absence of SPP waves.

To examine the scattering properties of SPP waves from an object, the backward-scattered fields in medium 1 are computed at $x = -0.5$ nm for both the incidence angle that excites the SPP waves, figure (3.4) (a) and (c), and the inci-

dence angle when the SPP waves are not excited; see figure (3.4) (b) and (d). Analysis is done on the impact of the size of the scatterer and its distance from the metal/medium 3 interface. An object close to the interface must scatter more than the one farther away since the SPP wave is localized to the interface. It is evident from the figure that when the SPP wave is excited compared to when it is not, the scattered field is far more prominent. The scattering enhancement is clearly noticed when the SPP waves propagate along the interface. The enhancement is at least of one order of magnitude. In the absence of the SPP wave the scattering amplitude is low. This simulation gives the idea of how far an object should be in order to avoid scattering effects in plasmonic communication. It can be deduced that the scattering effect can be neglected for the SPP wave propagation when the distance of the object with size $R = 5\ nm$ is $h = 100\ nm$. For a large object having $R = 20\ nm$, the scattering enhancement is large enough to be ignored.

The back scattered fields in figures (3.5) are computed for a corner reflector made of small circular scatterers to provide a better understanding of how SPP waves affect the scattered field, where the incidence angles are as indicated, $\theta_i = \theta_{\text{SPP}} = 22.9°$ and $\theta_i = 12.9°$. Analysis is done on the impact of the corner reflector size and its distance from the metal/medium 3 interface. Comparing the figures 3.5 (a), and (b) reveals that for the identical values of $L_1 = L_2$ and h, the backward-scattered field is ten times stronger when the SPP wave is present. From figures 3.5 (a) and (b), when h = 30 nm, the maximum value are 0.015 and 3×10^{-3} approximately. Comparing these values $0.015/3 \times 10^{-3} \approx 5$ times being less than one order of magnitude. This observation is also noted while we compare figure (3.5) (c) and (d). From figures (3.5) (c) and (d) when h = 100 nm the maximum value are 0.025 and 0.014 approximately. Comparing these values $0.025/0.014 \approx 2$ times being less than one order of magnitude. Since multiple objects are present, the scattering enhancement is larger than that was noticed for a single object. Multiple scattering occurs when a wave interacts with multiple objects, and the scattered waves interfere with each other. In general, the scattering enhancement due to multiple scattering is larger than that due to a single object. Once again low scattering can be seen when the SPP wave does not exist. This simulation helps in getting the

idea that how far a corner reflector can be placed to avoid scattering effects in plasmonic communication. For large object with $L_1 = L_2 = 30, 40$ *nm*, the scattering enhancement is observed to be very large.

(a) $L_1 = L_2 = 10$ nm, $\theta_i = \theta_{SPP} = 22.9°$

(b) $L_1 = L_2 = 10$ nm, $\theta_i = 12.9°$

(c) h = 100 nm, $\theta_i = \theta_{SPP} = 22.9°$

(d) h = 100 nm, $\theta_i = 12.9°$
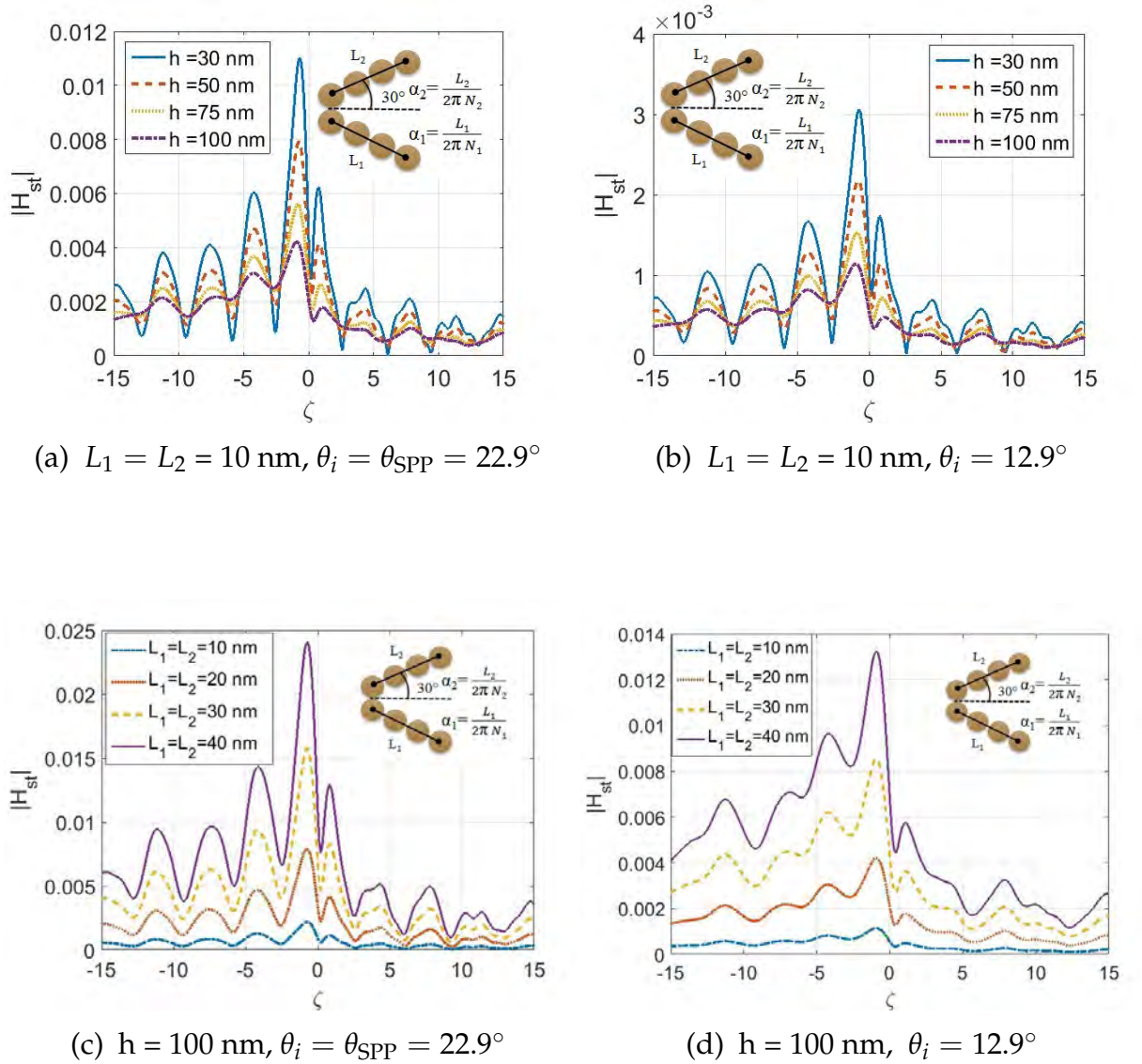
Figure 3.5: Enhancement in the scattered field due to SPP waves for a corner reflector, where $N_1 = N_2 = 4$ are the number of scatterers used to simulate a structure.

The simulation is done in figure (3.6) for a circular arrangement of small scatterers which mimics the metallic object of the circular cross section. Same area rule [161] is followed in these arrangements. For identical values of R and h, the scattered field is around 10 times stronger than when SPP wave is absent. Additionally, the scattered field becomes smaller as the size of the scatterer decreases or as it is moves away from the interface.

(a) $R = 10$ nm, $\theta_i = \theta_{SPP} = 22.9°$

(b) $R = 10$ nm, $\theta_i = 12.9°$

(c) $h = 100$ nm, $\theta_i = \theta_{SPP} = 22.9°$

(d) $h = 100$ nm, $\theta_i = 12.9°$
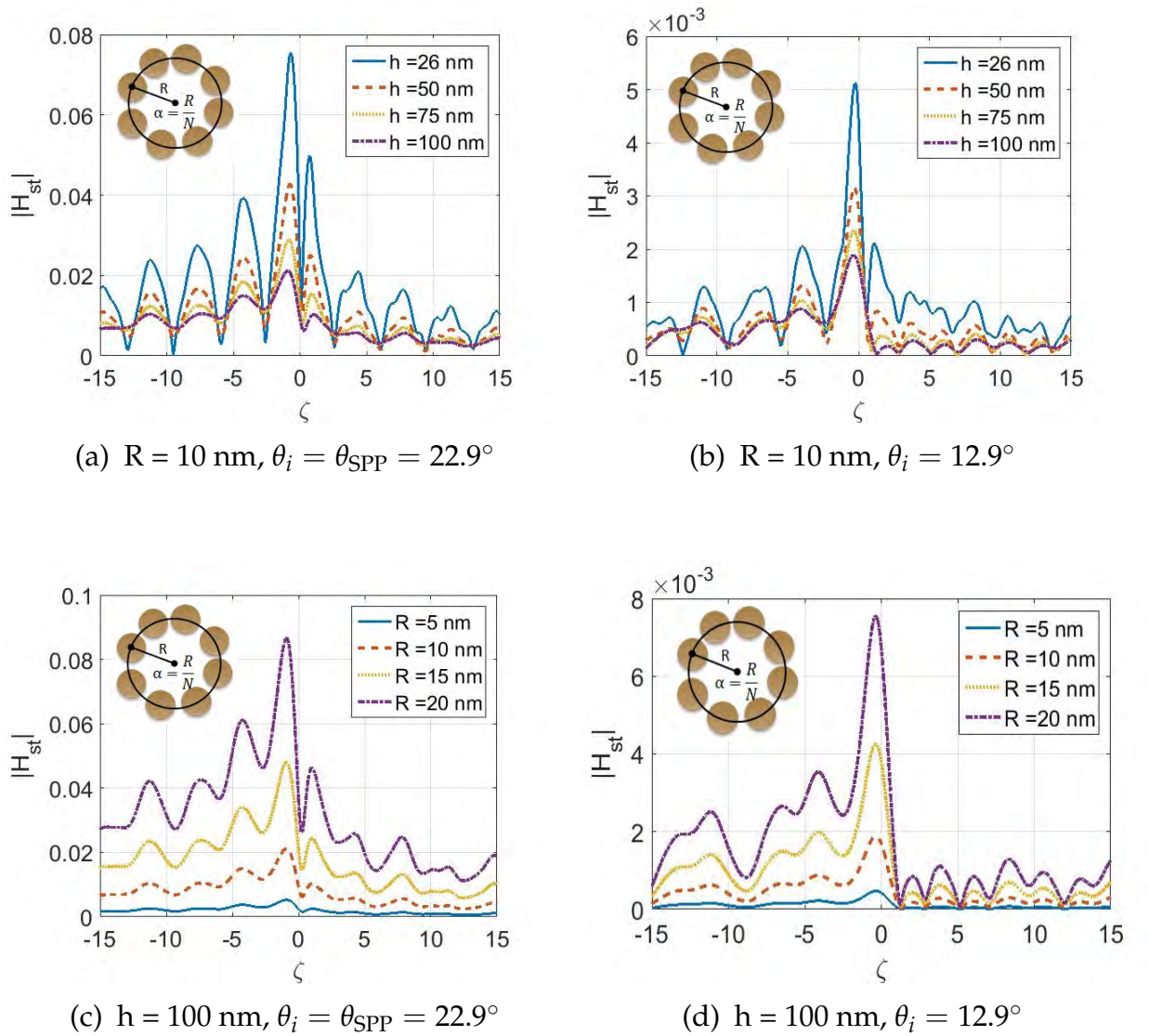
Figure 3.6: Effect of SPP waves on the scattered field of a circular object simulated by means of eight scatterers, N=8.

Now, we simulate a strip and the scattering behavior is shown in figure (3.7) for both scenarios when SPP wave excites and when it does not. A change in length L has a more substantial impact on the scattered field, than a change in the depth of the structure. As the length increases, its scattering surface expands which results in increasing the energy of the excitations of the scatterer. The placement of a strip in the system for plasmonic communication is more affected by the scattering enhancement due to SPP waves.

(a) L = 10 nm, $\theta_i = \theta_{\text{SPP}} = 22.9°$

(b) L = 10 nm, $\theta_i = 12.9°$

(c) h = 100 nm, $\theta_i = \theta_{\text{SPP}} = 22.9°$

(d) h = 100 nm, $\theta_i = 12.9°$
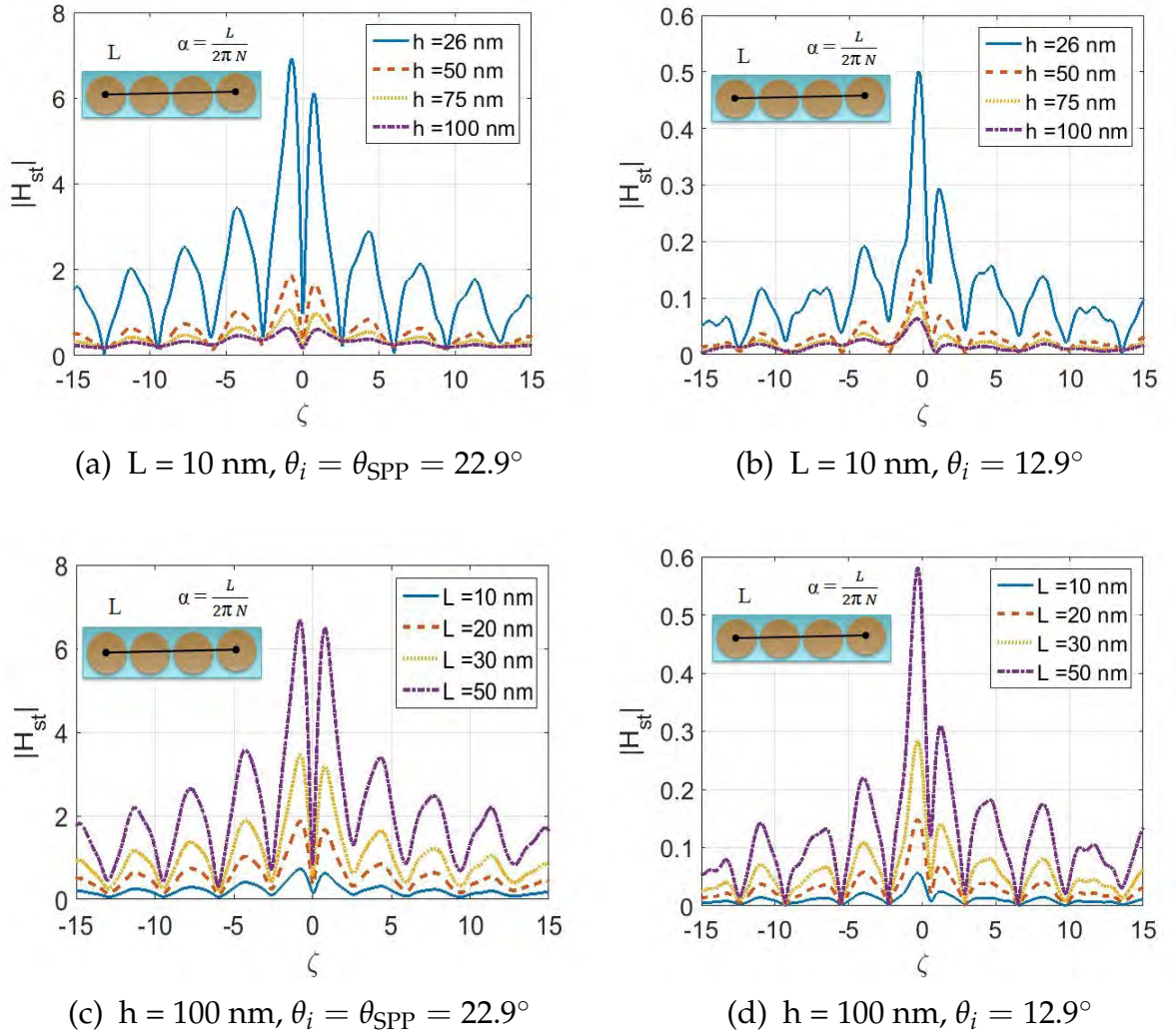
Figure 3.7: Intensified scattered field in the presence of SPP waves for a strip simulated by the placement of small scatterers, where N = 4.

In addition to the backward scattered fields, two-dimensional field maps are more helpful to analyze the field in the vicinity of the object as demonstrated in figure (3.8). Unlike usual scattering for a plane wave incidence from medium 1, the amplitude on both sides of the scatterer is high in the presence of the SPP waves rather than on the upper side from which the object is illuminated. Effectively, when a surface plasmon is excited on the interface between a metal and a dielectric, the electric field amplitude at the interface can be significantly enhanced. The enhancement of the electric field amplitude is due to the coupling between the surface plasmon and the incident electromagnetic wave and being high in medium 3 where the wave has large penetration length. Backscattered field is very low compared to field on both edges of the object. The scattering of SPPs due to interaction with a corner reflector depends on the angle of incidence and the shape of the reflector. For this configuration, when the angle of incidence is small, the scattering from the apex of a corner reflector is stronger than that from the edge. A dipole like field is present at the edges of the corner reflector as presented in figure (3.8a), and also at the edges of the strip in figure (3.8b). The dipole-like distribution is due to the interference between the scattered waves from adjacent spheres, where the interference leads to constructive and destructive interference patterns, which result in the dipole-like distribution of the electric field. The near zone scattered field is shown when scatterers are arranged in a circular form in figure (3.8c). Once again it is evident that the field strength is strong on the right and left sides of the object rather than back/forward scattering due to SPP wave excitation.

From the simulated results, it can be anticipated that SPP scattering can interfere destructively with direct SPP wave transmission and this can cause a strong interruption at the receiver. In addition, SPP wave scattering will definitely reach the receiver as it is very strong when the scatterer is placed near the interface.

(a) $L_1 = L_2 = 20$ nm, h = 32 nm

(b) $L = 20$ nm, h = 20 nm,

(c) R = 5 nm, h = 27 nm
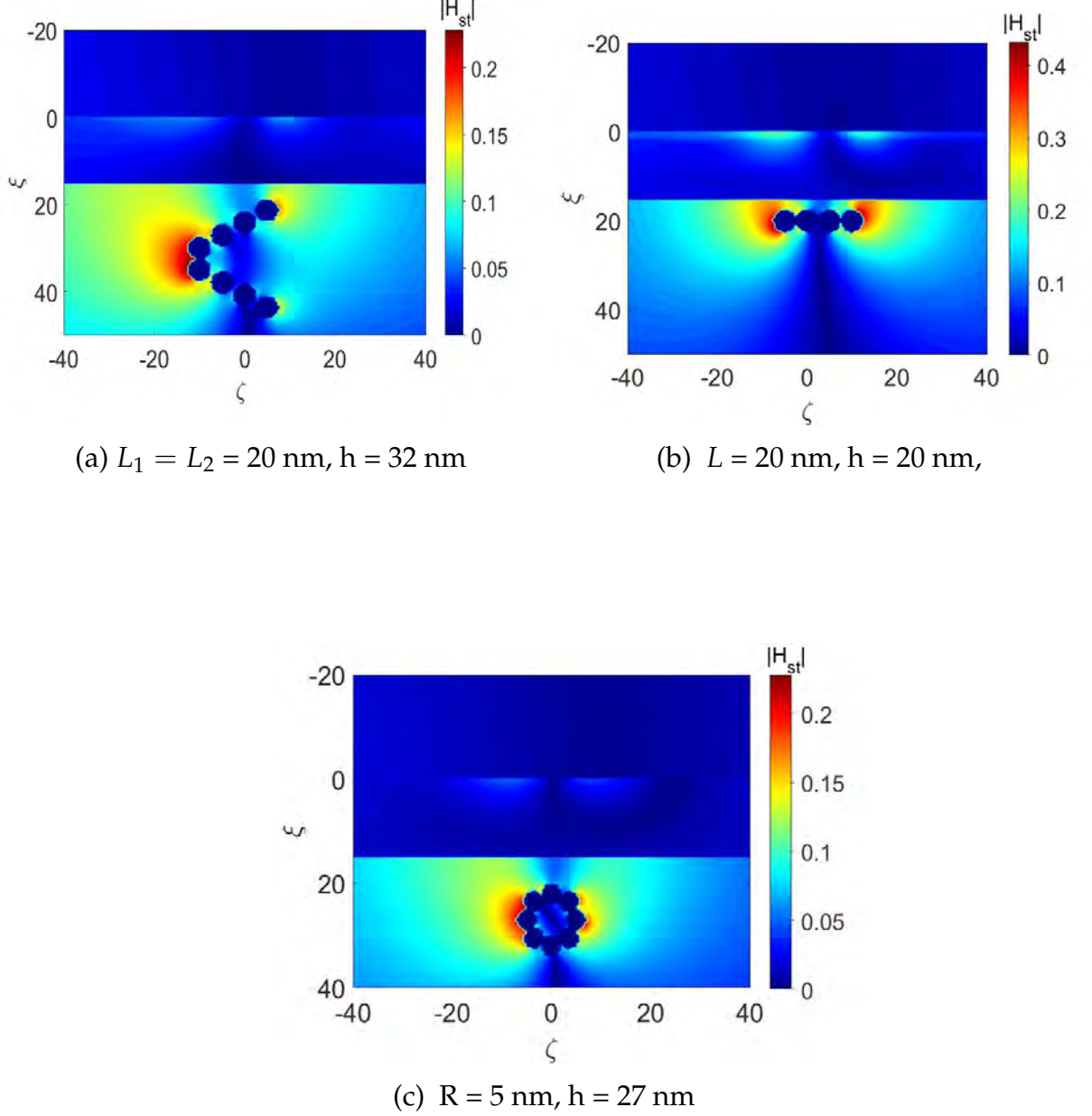
Figure 3.8: (a) Two-dimensional maps of intensified scattered fields of a corner reflector, (b) scatterers arranged in a strip form, and (c) a circular arrangement of small scatterers which mimics the perfectly conducting object, where $\theta_i = \theta_{spp} = 22.9°$, and angle of corner reflector is 30°.

Chapter 4

Scattering of SPP waves excited by grating coupled configuration

This chapter analyzes the scattering of SPP waves excited by using the grating coupled configuration. The reflection and transmission coefficients of a grating can be obtained using EBCM [162] discussed in chapter 2. The metallic circular scatterer is considered. The grating formulation is combined with the CWA approach to analyze the SPP wave scattering and signal distortion. In section (4.1) problem description and formulation are given, while in section (4.2) numerical results are reported.

4.1 Problem description and formulation

The geometry of the problem is shown in figure (4.1). The permittivity and permeability of free space are ϵ_o and μ_o, respectively, while ϵ_1 and μ_1 are the permittivity and permeability of the host medium, respectively. Two reference frames are introduced. The main reference frame (MRF) $(0, \xi, \zeta)$ with normalized coordinates $\xi = k_o x$, $\zeta = k_o\, z$, and the reference frame centered on the scatterer (RF_q) (ξ_q, ζ_q) with normalized coordinates $\xi_q = \xi - \chi_q$, $\zeta_q = \xi - \eta_q$ are assumed. The scatterer has a normalized size $\alpha_q = k_o a$ and is placed at MRF i.e., $(\chi_q = k_o\, d, \eta_q)$, where χ_q is the normalized distance of the metallic scatterer from the interface and k_o is the wave number of free space. The time

Figure 4.1: Geometry of the problem

dependency e^{-jwt} is considered.

Table 4.1: The involved fields in each medium.

Field components	Descriptions
$V_i(\xi,\zeta)$	Incident plane wave at region 0
$V_r(\xi,\zeta)$	Reflected plane wave at region 0
$V_t(\xi,\zeta)$	Transmitted plane wave to region 1
$V_s(\xi,\zeta)$	Scattered field from metallic circular scatterer
$V_{sr}(\xi,\zeta)$	Scattered reflected field from scatterer and grating
$V_{st}(\xi,\zeta)$	Scattered transmitted field into region 0

According to cylindrical scattering problems, the convention for polarizations such as TE/TM is used when the electric/magnetic field is transverse to the axis of the scatterer as

$$V(\xi,\zeta) = E_y(\xi,\zeta), \quad \text{TM-Polarization}$$
$$V(\xi,\zeta) = H_y(\xi,\zeta), \quad \text{TE-Polarization}$$

The $V(\xi, \zeta)$ function represents the multiple field contributions in each medium due to the incident field. The primary reflection from the grating can be written as [97]

$$V_r(\xi, \zeta) = V_0 \frac{1}{2\pi} \int_{-\infty}^{\infty} \gamma_{01s}(n_{\parallel}) e^{j(-n_{\perp}\xi + n_{\parallel}\zeta)} dn_{\parallel} \tag{4.1}$$

Here, $\gamma_{01s}(n_{\parallel})$ is the reflection coefficient that represents the field from the flat interface and grating contributions. For flat $\gamma_{01s}(n_{\parallel})$, s=0, while for grating contribution, $s = \pm 1, \pm 2$ and so on. The field penetrated into region 1 is described as [97]

$$V_t(\xi, \zeta) = V_0 \frac{1}{2\pi} \int_{-\infty}^{\infty} \tau_{01s}(n_{\parallel}) e^{jn_1(n_{\perp}\chi_q + n_{\parallel}\eta_q)} e^{jn_1(n_{\perp}\xi_q + n_{\parallel}\zeta_q)} dn_{\parallel} \tag{4.2}$$

The transmitted field will be incident upon a metallic circular object. In a polar coordinate system, it can be written as

$$V_t(\xi_q, \zeta_q) = V_0 \sum_{\ell=-\infty}^{\infty} j^{\ell} J_{\ell}(n_1 \rho_q) e^{j\ell\theta_q} \times \triangle B \tag{4.3}$$

where

$$\triangle B = \frac{1}{2\pi} \int_{-\infty}^{\infty} \tau_{01s}(n_{\parallel}) e^{jn_1(n_{\perp}\chi_q + n_{\parallel}\eta_q)} e^{-j\ell \tan^{-1}(\frac{n_{\parallel}}{n_{\perp}})} dn_{\parallel} \tag{4.4}$$

The scattered field can be represented as a sum of cylindrical functions $CW_m(n_1\xi_q, n_1\zeta_q) = H_m^1(n_1\rho_q) e^{jm\theta_q}$, where H_m^1 is a first-kind Hankel function of order m. Therefore, we have

$$V_s(\xi, \zeta) = V_0 \sum_{m=-\infty}^{\infty} j^m c_{qm} CW_m(n_1\xi_q, n_1\zeta_q) e^{-jm\theta_t} \tag{4.5}$$

where

$$CW_m(\xi, \zeta) = \frac{1}{2\pi} \int_{-\infty}^{\infty} F_m(\xi, n_{\parallel}) e^{jn_{\parallel}\zeta} dn_{\parallel} \tag{4.6}$$

The Fourier spectrum of $F_m(\xi, n_\parallel)$ may be written as [163]

$$F_m(\xi, n_\parallel) = \frac{2e^{j|\zeta|}\sqrt{1-n_\parallel^2}}{1-n_\parallel^2} \begin{cases} e^{-jm\arccos n_\parallel}, & \xi \leq 0, \\ e^{jm\arccos n_\parallel}, & \xi \geq 0, \end{cases} \tag{4.7}$$

The scattered-reflected field comprises all field configurations resulting from the reflection of each cylindrical wave from a grating. The scattered-reflected field is [97]

$$V_{sr}(\xi, \zeta) = V_0 \sum_{m=-\infty}^{\infty} j^m e^{-jm\theta_t} c_{qm} RW_m[n_1(-\xi_q - 2\chi_q), n_1\zeta_q, \chi_q] \tag{4.8}$$

where RW_m is the reflected cylindrical function of order m can be written as

$$RW_m(\xi, \zeta, \chi) = RW_m^0(\xi, \zeta) + RW_m^s(\xi, \zeta, \chi) \tag{4.9}$$

where the expressions of RW_m^0 and RW_m^s are given as

$$RW_m^0(\xi, \zeta) = \frac{1}{2\pi} \int_{-\infty}^{\infty} \gamma_{10s}(n_\parallel) F_m(\xi, n_\parallel) e^{jn_\parallel} dn_\parallel \tag{4.10}$$

$$RW_s^s(\xi, \zeta, \chi) = \frac{1}{(2\pi)^2} \int_{-\infty}^{\infty} \int_{-\infty}^{\infty} \gamma_{10s}(n_\parallel', n_\parallel)$$
$$\times F_m(-n_1\chi, n_\parallel) e^{j(n_\perp' \xi + n_\parallel' \zeta)} dn_\parallel dn_\parallel' \tag{4.11}$$

Equations (4.10) and (4.11) use reflection coefficients $\gamma_{10s}(n_\parallel)$ and $\gamma_{10s}(n_\parallel', n_\parallel)$, which are similar to equation (4.1), but with a reversed propagation from medium 1 to medium 0 taken into account. It is worth noting that in equation (4.10), the reflection coefficient represents the zeroth order and s = 0. On the other hand, in equation (4.11), s = $\pm 1, \pm 2$, and so on, representing the grating components. Starting from equation (4.8), making use of (4.7) in (4.10) and (4.11), and of the expansion of a plane wave into the Bessel functions, the following expression

of the field $V_{sr}(\xi, \zeta)$ is obtained

$$
V_{sr}(\xi, \zeta) = V_0 \sum_{\ell=-\infty}^{\infty} J_\ell(n_1 \rho_q) e^{j\ell\theta_q} \sum_{m=-\infty}^{\infty} j^m e^{-jm\theta_t} \times
$$
$$
c_{qm}[RW_{m+\ell}^0(-2n_1\chi_q, 0) + RW_{m,\ell}^s(-n_1\chi_q, 0, \chi_q)] \tag{4.12}
$$

The expressions of $RW_m^0(-2n_1\chi_q, 0)$ and $RW_m^s(-n_1\chi_q, 0, \chi_q)$ are given as

$$
RW_{m+\ell}^0(-2n_1\chi_q, 0) = \frac{1}{2\pi} \int_{-\infty}^{\infty} \gamma_{10s}(n_\parallel) F_m(-2n_1\chi_q, n_\parallel) e^{jn_\parallel} dn_\parallel \tag{4.13}
$$
$$
RW_{m,\ell}^s(-n_1\chi_q, 0, \chi_q) = \frac{1}{(2\pi)^2} \int_{-\infty}^{\infty} \int_{-\infty}^{\infty} \gamma_{10s}(n_\parallel', n_\parallel)
$$
$$
\times F_m(-n_1\chi_q, n_\parallel) e^{-jn_\perp'\chi_q} e^{-j\ell\theta_{sr}} dn_\parallel dn_\parallel' \tag{4.14}
$$

The scattered transmitted field, expressed in terms of the transmitted cylindrical wave function $TW_m(\xi, \zeta, \chi)$, can be written as:

$$
V_{st}(\xi, \zeta) = V_0 \sum_{m=-\infty}^{\infty} j^m e^{-jm\theta_t} c_{qm} TW_m(\xi - \chi_q, \zeta - \eta_q, \chi_q) \tag{4.15}
$$

where

$$
TW_m(\xi, \zeta, \chi) = TW_m^0(\xi, \zeta, \chi) + TW_m^s(\xi, \zeta, \chi) \tag{4.16}
$$

The explicit expressions of $TW_m^0(\xi, \zeta, \chi)$ and $TW_m^s(\xi, \zeta, \chi)$ are given

$$
TW_m^0(\xi, \zeta, \chi) = \frac{1}{2\pi} \int_{-\infty}^{\infty} \tau_{10s}(n_\parallel)
$$
$$
\times F_m(-n_1\chi, n_\parallel) e^{-j\sqrt{1-(n_\perp n_\parallel)^2}(\xi+\chi)} e^{jn_\perp n_\parallel \zeta} dn_\parallel \tag{4.17}
$$
$$
TW_m^s(\xi, \zeta, \chi) = \frac{1}{(2\pi)^2} \int_{-\infty}^{\infty} \int_{-\infty}^{\infty}
$$
$$
\times \tau_{10s}(n_\parallel', n_\parallel) F_m(-n_1\chi, n_\parallel) e^{-j\sqrt{1-(n_1 n_\parallel')^2}(\xi+\chi)} e^{jn_1 n_\parallel' \zeta} dn_\parallel dn_\parallel' \tag{4.18}
$$

The transmission coefficients from medium 1 to medium 0 are represented by $\tau_{10s}(n_\parallel)$ and $\tau_{10s}(n_\parallel', n_\parallel)$. In equation (4.17), s = 0, while in equation (4.18), s = $\pm 1, \pm 2$, and so on. Applying the boundary condition at $\rho_p = \alpha_p$ on the surface

of the scatterer for both polarizations, we get

$$V_t + V_s + V_{sr} \mid_{\rho_p = \alpha_p} = 0 \qquad \text{TM - polarization}$$

$$\frac{\partial}{\partial \rho_p}(V_t + V_s + V_{sr}) \mid_{\rho'_p = \alpha_p} = 0 \quad \text{TE - polarization}$$

$$(4.19)$$

By putting the equations (4.3), (4.5) and (4.12) in equation (4.19) we get [97]

$$\sum_{m=-\infty}^{\infty} A_{m\ell}^{qp(TM,TE)} c_{qm} = B_{\ell}^{p(TM,TE)}, \quad \{\ell = 0, \pm 1, \pm 2 ..... \pm \infty \tag{4.20}$$

$$A_{\ell m}^{qp(TM,TE)} = j^{m-\ell} e^{-jm\theta_t} [RW_{m+\ell}^0(-2n_1\chi_q, 0) + RW_{m,\ell}^s(-n_1\chi_q, 0)]$$

$$\times G_{\ell}^{(TM,TE)}(n_1\alpha_q) + \delta_{m\ell} \tag{4.21}$$

and

$$B_{\ell}^{p(TM,TE)} = -G_{\ell}^{(TM,TE)}(n_1\alpha_p) \left\{ \tau_{01p}(n_{\parallel}^i) e^{j(n_{\perp}^t \chi_q + n_{\parallel}^t \eta_q)} e^{-j\ell\theta_{t1}} + \triangle B \right\} \tag{4.22}$$

where δ_{ml} is the Kronecker delta function and

$$G_{\ell}^{(TM)} = \frac{J_{\ell}(x)}{H_{\ell}^{(1)}(x)} \tag{4.23}$$

$$G_{\ell}^{(TE)} = \frac{J_{\ell}'(x)}{H_{\ell}'^{(1)}(x)} \tag{4.24}$$

4.2   Results and discussion

First, we compare the formulation with results obtained by CWA [97] shown in figure (4.2). The scattering cross section $\sigma[dB]$ is plotted with respect to the scattered angle. The simulation parameters used to obtain the result are h = 0.0064 λ_0, $\epsilon_1 = 4\epsilon_0$, $P_s = 0.8\pi$, χ_q=2.6 π, $\alpha_q = 0.32\pi$, $\theta_i = 30°$, and $\eta_q = 0$.

The effect of SPP waves on the scattering for a metallic circular scatterer for different values of size is reported in figure (4.3). The simulation parameters are $\epsilon_1 = -7.0410 + 0.2781j$, $\lambda = 633$ nm, $P_s = 1100$ nm, and h = 100 nm. The

grating is coated with silver. It is evident from the figures that the scattered field increases with increasing size of the scatterer. Additionally, the scattered field intensity is much higher when the incident angle is equal to θ_{SPP} than when the incident angle is not an SPP.

In figure (4.4) the scattered field is observed when the scattered is placed at different distance values from the grating. The simulation parameters are $\epsilon_1 = -7.0410 + 0.2781j$, $\lambda = 633$ nm, $P_s = 1100$ nm and h = 100 nm. It has been observed that the scattered field reduces as the object moves away from the grating. It highlights that the presence of SPP waves near the interface is much stronger than away from the interface. The amplitude of the scattered field is higher when the incident angle is θ_{SPP} than when it is not.

In figure (4.5) the effect of the period on the scattered field is analyzed. The simulation parameters used to obtain the results are $\epsilon_1 = -7.0410 + 0.2781j$, a = 20 nm, d = 26 nm, $\lambda = 633$ nm, and h = 100 nm. The side and main lobes change by increasing the period from 900 nm to 1700 nm. Moreover, the side lobe (peaks) is stronger than the central lobe. The same pattern is observed with the use of incident angle $\theta_i = \theta_{SPP} = 25.5°, 46.7°$ and once again the field intensity is higher than the intensity when the angle of incident is not an θ_{SPP}.

In the end, the scattered field for different values of the grating height is plotted with respect to the scattered angle in figure (4.6). The $\epsilon_1 = -7.0410 + 0.2781j$, a = 20 nm, d = 26 nm, $\lambda = 633$ nm, and $P_s = 1200$ nm are the simulation parameters. The scattered field increases with an increase in the height of the grating. Moreover, the scattered field is small when the angle of the incident is not equal to θ_{SPP}.

From the above analysis, it is evident that the signal propagation will be interrupted by the presence of a strong scattered field. Interference of SPP wave propagation with scattered fields is quite obvious. Moreover, the reception of SPP scattering at the receiver is another factor that will distort the information sent to the receiver. The simulated scenarios help in determining the combination of size and distance which does not distort the signal propagation due to scattering effects. This simulation gives an idea of how far an object should be in order to avoid scattering effects in plasmonic communication.
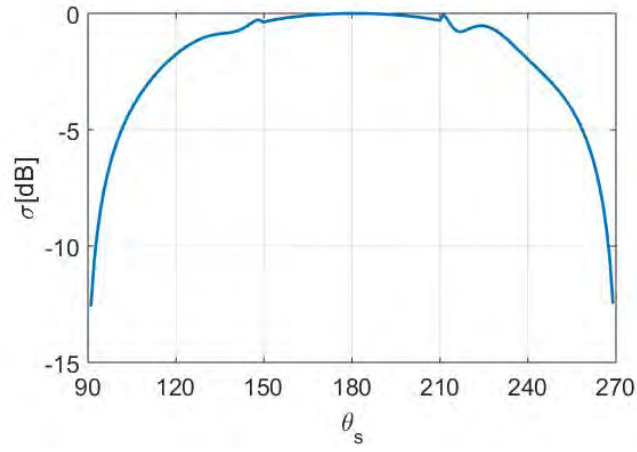
Figure 4.2: The scattering cross section σ is plotted as a function of scattered angle. The simulation parameters are h = 0.0064 λ_0, $n_1 = 2$, $P_s = 0.8\pi$, χ_q=2.6 π, $\alpha_q = 0.32\pi$, $\theta_i = 30°$, and $\eta_q = 0$.
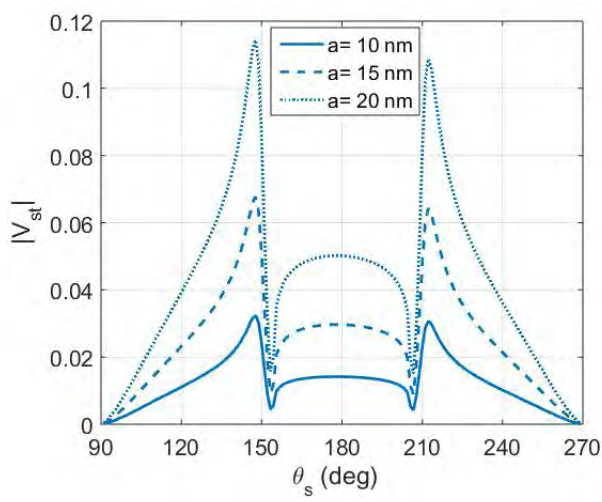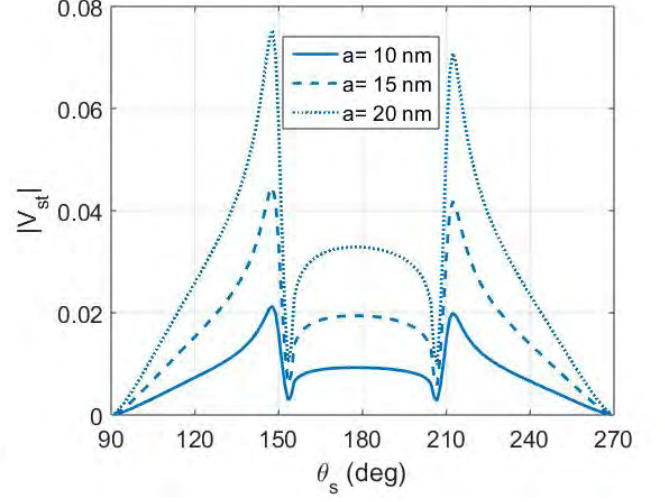
(a) d = 26 nm, $\theta_i = \theta_{\text{SPP}} = 33^o$

(b) d = 26 nm, $\theta_i = 43^o$
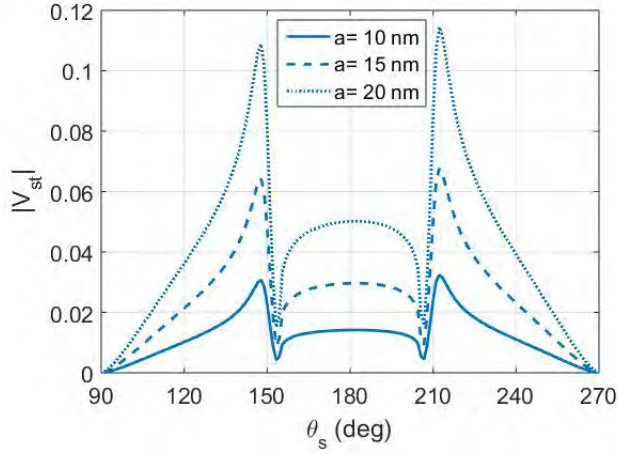
(c) d = 26 nm, $\theta_i = \theta_{\text{SPP}} = -33^o$
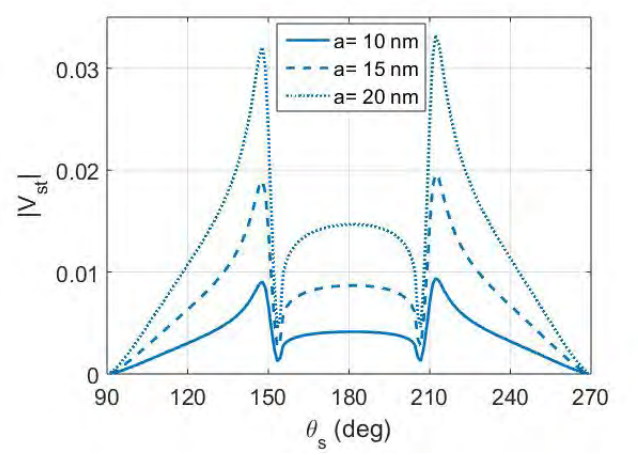
(d) d = 26 nm, $\theta_i = -23^o$

Figure 4.3: Effect of SPP waves on the scattered field for a metallic circular scatterer. The parameters are $\epsilon_1 = -7.0410 + 0.2781j$, $\lambda = 633$ nm, $P_s = 1100$ nm and h = 100 nm. The grating is coated with silver.
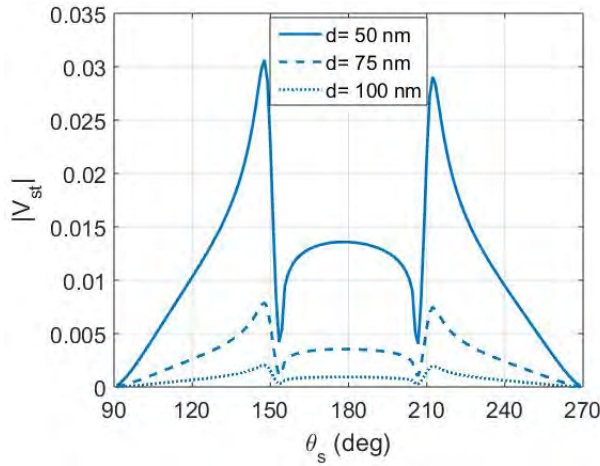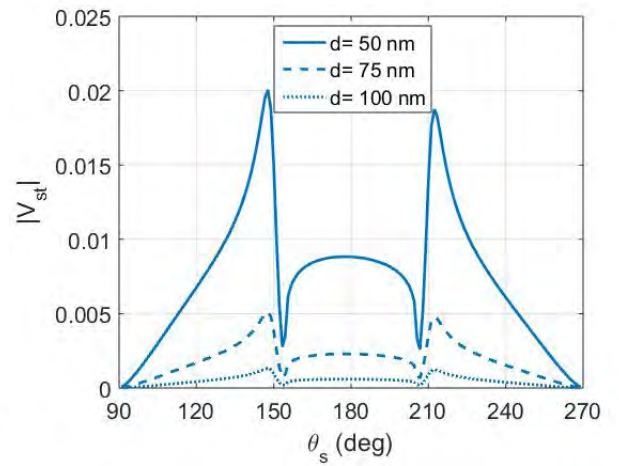
(a) a = 20 nm, $\theta_i = \theta_{\text{SPP}} = 33^o$

(b) a = 20 nm, $\theta_i = 43^o$
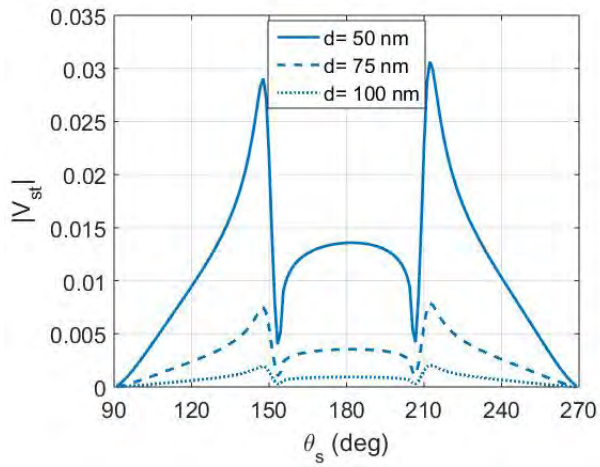
(c) a = 20 nm, $\theta_i = \theta_{\text{SPP}} = -33^o$
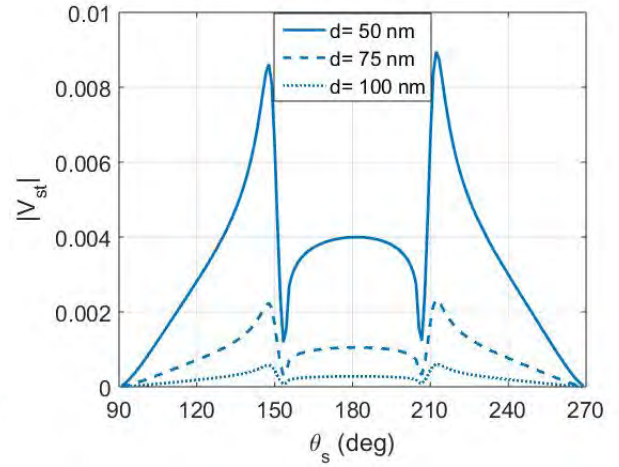
(d) a = 20 nm, $\theta_i = -23^o$

Figure 4.4: Scattered field for different values of distance of scatterer from the grating. The parameters are $\epsilon_1 = -7.0410 + 0.2781j$, $\lambda = 633$ nm, $P_s = 1100$ nm and h = 100 nm.
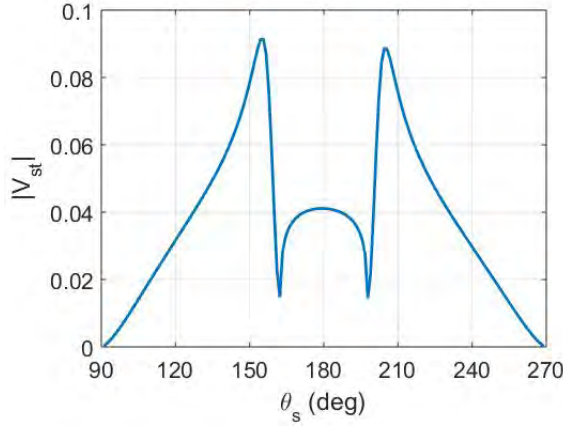
(a) P_s = 900 nm, $\theta_i = \theta_{SPP} = 25.5^o$
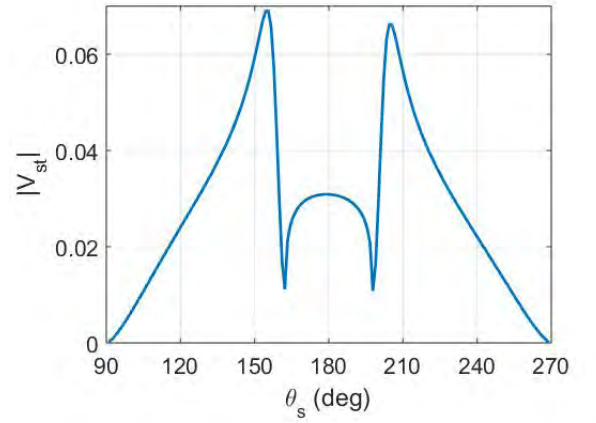
(b) P_s = 900 nm, $\theta_i = 35.5^o$
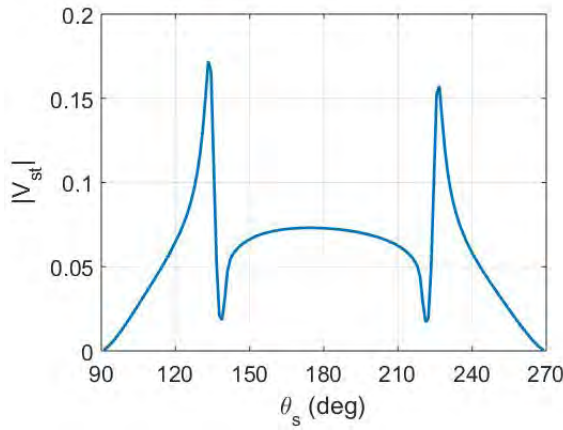
(c) P_s = 1700 nm, $\theta_i = \theta_{SPP} = 46.7^o$
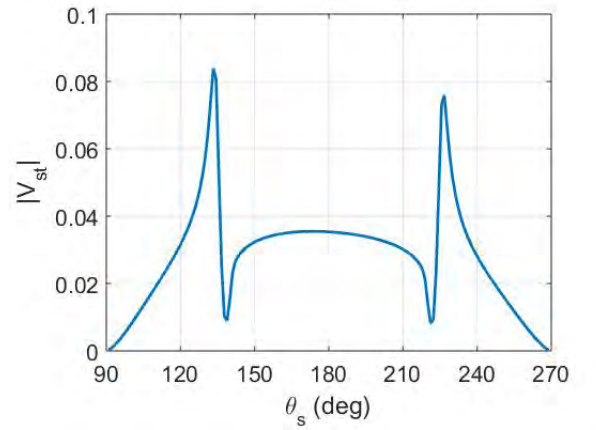
(d) P_s = 1700 nm, $\theta_i = 56.7^o$

Figure 4.5: The effect of the period on the scattered field in the presence and absence of SPP wave, where the simulation parameters are $\epsilon_1 = -7.0410 + 0.2781j$, a = 20 nm, d = 26 nm, $\lambda = 633$ nm, and h = 100 nm.
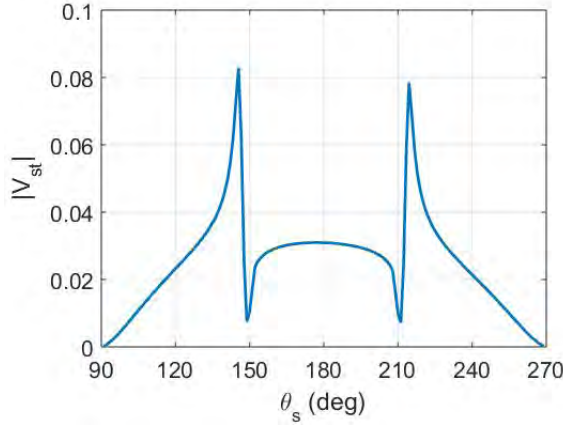
(a) h = 70 nm, $\theta_i = \theta_{SPP} = 34.6^o$
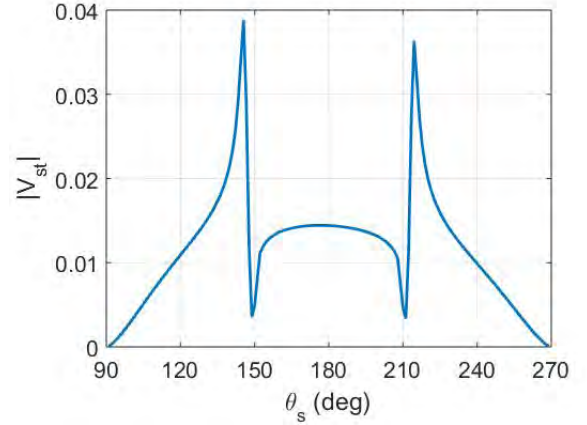
(b) h = 70 nm, $\theta_i = 44.6^o$
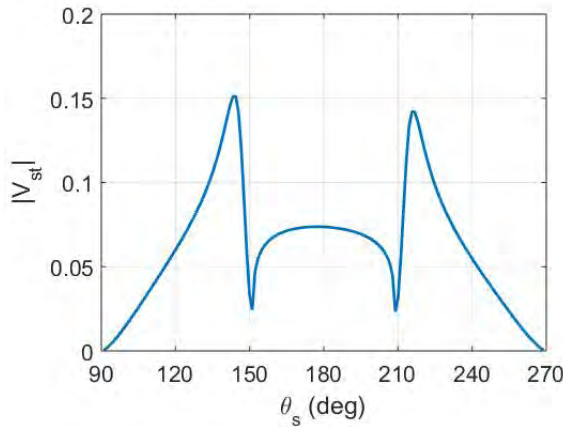
(c) h = 120 nm, $\theta_i = \theta_{SPP} = 37.3^o$
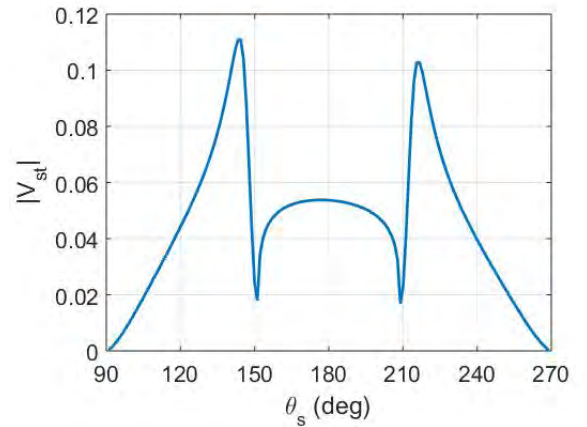
(d) h = 120 nm, $\theta_i = 47.3^o$

Figure 4.6: Variation of the scattered field by changing the height of the grating in the presence and absence of SPP wave. The parameters are $\epsilon_1 = -7.0410 + 0.2781j$, a = 20 nm, d = 26 nm, $\lambda = 633$ nm, and $P_s = 1200$ nm.

Chapter 5

Conclusions

Effect of SPP waves on scattering phenomenon from cylindrical structures such as a corner reflector and a strip is analyzed using the cylindrical wave approach. A comparison is presented between scattered field when the SPP waves are excited and when the SPP waves are not excited. Different arrangements are simulated by means of multiple metallic circular scatterers. It is noted that the scattered field from the strip is very strong and can be one of the major challenges in plasmonic communication due to strong scattering losses. The enhancement of the electric field amplitude is due to the coupling between the surface plasmon and the incident electromagnetic wave. Moreover, the simulations give the idea that what structure size and distance from the interface do not produce significant scattering. The backward-scattered field by a corner reflector is ten times stronger when the SPP wave is present.

To observe the field in the vicinity of the object, two-dimensional near zone field maps are presented which show dipole-like scattering due to SPP wave excitation unlike usual scattering for a plane wave excitation. The placement of a strip near another configuration/element in an on-chip plasmonic communication system can be a major challenge as the scattering field is strong on both edges. This issue also arises for a corner reflector with a strong field near the corner and edges. The application of SPPs in on-chip communications encounters challenges due to scattering losses during signal transmission. These losses can lead to adverse effects such as power reduction and distortion of the pulse shape, impacting the overall integrity and strength of the transmitted

signals. In order to build plasmonic communication applications, it is critical to first understand the scattering mechanisms and properties.

In a second problem, the scattering of SPP waves excited by grating from a metallic circular scatterer is described. The extended boundary condition method (EBCM) is utilized to derive the reflection and transmission coefficients. In the first step, the angles of exciting SPP (θ_{SPP}) are measured by plotting the reflection coefficient square ($|\gamma_{01n}|^2$).

The numerical results are reported for different values of the sizes and distances of the scatterer from the grating. It has been observed that the scattered field increases as the size of the scatter increases. Additionally, the scattered field intensity is much higher when the angle of incident is equal to the angle of excitation of SPP than when the angle of incident is not SPP.

The scattered field reduces with increase in the distance of the scatterer from the grating which shows that the effect of SPP waves near the interface is much stronger than away from the interface. The amplitude of the scattered field is higher when the incident angle is θ_{SPP}, than when it is not.

The effect of the period and height on the scattered field is also analyzed. It has been noticed that the scattered field increases with an increase in the height of the grating. The scattered field is smaller when the angle of the incident is not θ_{SPP}.

From the simulated results, it can be anticipated that SPP scattering can interfere destructively with direct SPP wave transmission and this can cause a strong interruption at the receiver. In addition, SPP wave scattering will definitely reach the receiver as it is very strong when the scatterer is placed near the interface.

Bibliography

[1] Josh A Conway, Subal Sahni, and Thomas Szkopek. Plasmonic interconnects versus conventional interconnects: a comparison of latency, crosstalk and energy costs. *Optics Express*, 15(8):4474–4484, 2007.

[2] Stefan A Maier. Plasmonics: The promise of highly integrated optical devices. *IEEE Journal of Selected Topics in Quantum Electronics*, 12(6):1671–1677, 2006.

[3] Harry A Atwater. The promise of plasmonics. *Scientific American*, 296(4):56–63, 2007.

[4] John B Pendry, David Schurig, and David R Smith. Controlling electromagnetic fields. *Science*, 312(5781):1780–1782, 2006.

[5] Vladimir M Shalaev. Optical negative-index metamaterials. *Nature Photonics*, 1(1):41–48, 2007.

[6] Katrin Kneipp, Yang Wang, Harald Kneipp, Lev T Perelman, Irving Itzkan, Ramachandra R Dasari, and Michael S Feld. Single molecule detection using surface-enhanced Raman scattering (SERS). *Physical Review Letters*, 78(9):1667, 1997.

[7] Hongxing Xu, Javier Aizpurua, Mikael Käll, and Peter Apell. Electromagnetic contributions to single-molecule sensitivity in surface-enhanced Raman scattering. *Physical Review E*, 62(3):4318, 2000.

[8] Prashant K Jain, Ivan H El-Sayed, and Mostafa A El-Sayed. Au nanoparticles target cancer. *Nano Today*, 2(1):18–29, 2007.

[9] Stefan Enoch, Romain Quidant, and Gonçal Badenes. Optical sensing based on plasmon coupling in nanoparticle arrays. *Optics Express*, 12(15):3422–3427, 2004.

[10] Jagmeet Singh Sekhon and SS Verma. Optimal dimensions of gold nanorod for plasmonic nanosensors. *Plasmonics*, 6:163–169, 2011.

[11] Jagmeet Singh Sekhon and S S Verma. Refractive index sensitivity analysis of ag, au, and cu nanoparticles. *Plasmonics*, 6:311–317, 2011.

[12] Anatoly V Zayats and Igor I Smolyaninov. Near-field photonics: surface plasmon polaritons and localized surface plasmons. *Journal of Optics A: Pure and Applied Optics*, 5(4):S16, 2003.

[13] William L Barnes, Alain Dereux, and Thomas W Ebbesen. Surface plasmon subwavelength optics. *Nature*, 424(6950):824–830, 2003.

[14] Domenico Pacifici, Henri J Lezec, and Harry A Atwater. All-optical modulation by plasmonic excitation of cdse quantum dots. *Nature Photonics*, 1(7):402–406, 2007.

[15] Kevin F MacDonald and Nikolay I Zheludev. Active plasmonics: current status. *Laser & Photonics Reviews*, 4(4):562–567, 2010.

[16] Shan Wu, Zhao Zhang, Yi Zhang, Kaiyin Zhang, Lin Zhou, Xuejin Zhang, and Yongyuan Zhu. Enhanced rotation of the polarization of a light beam transmitted through a silver film with an array of perforated s-shaped holes. *Physical Review Letters*, 110(20):207401, 2013.

[17] Rupert F Oulton, Volker J Sorger, DA Genov, DFP Pile, and X Zhang. A hybrid plasmonic waveguide for subwavelength confinement and long-range propagation. *Nature Photonics*, 2(8):496–500, 2008.

[18] Takuo Tanemura, Krishna C Balram, Dany-Sebastien Ly-Gagnon, Pierre Wahl, Justin S White, Mark L Brongersma, and David AB Miller. Multiple-wavelength focusing of surface plasmons with a nonperiodic nanoslit coupler. *Nano Letters*, 11(7):2693–2698, 2011.

[19] Xiaowei Li, Qiaofeng Tan, Benfeng Bai, and Guofan Jin. Non-spectroscopic refractometric nanosensor based on a tilted slit-groove plasmonic interferometer. *Optics Express*, 19(21):20691–20703, 2011.

[20] Yulan Fu, Xiaoyong Hu, Cuicui Lu, Song Yue, Hong Yang, and Qihuang Gong. All-optical logic gates based on nanoscale plasmonic slot waveguides. *Nano Letters*, 12(11):5784–5790, 2012.

[21] Jianjun Chen, Zhi Li, Jia Li, and Qihuang Gong. Compact and high-resolution plasmonic wavelength demultiplexers based on fano interference. *Optics Express*, 19(10):9976–9985, 2011.

[22] Aaron Hryciw, Young Chul Jun, and Mark L Brongersma. Electrifying plasmonics on silicon. *Nature Materials*, 9(1):3–4, 2010.

[23] S Pillai, , and MA Green. Plasmonics for photovoltaic applications. *Solar Energy Materials and Solar Cells*, 94(9):1481–1486, 2010.

[24] Harry A Atwater and Albert Polman. Plasmonics for improved photovoltaic devices. *Nature Materials*, 9(3):205–213, 2010.

[25] Syed Mubeen, Joun Lee, Woo-ram Lee, Nirala Singh, Galen D Stucky, and Martin Moskovits. On the plasmonic photovoltaic. *ACS Nano*, 8(6):6066–6073, 2014.

[26] Nikolay L Kazanskiy, Muhammad A Butt, and Svetlana N Khonina. Optical computing: Status and perspectives. *Nanomaterials*, 12(13):2171, 2022.

[27] William O F. Carvalho and J Ricardo Mejía-Salazar. Plasmonics for telecommunications applications. *Sensors*, 20(9):2488, 2020.

[28] Anand M Shrivastav, Uroš Cvelbar, and Ibrahim Abdulhalim. A comprehensive review on plasmonic-based biosensors used in viral diagnostics. *Communications Biology*, 4(1):70, 2021.

[29] Juerg Leuthold, Yannik Horst, Tobias Blatter, Laurenz Kulmer, Loïc Chérix, David Moor, Marco Eppenberger, Michael Baumann, Stefan M

Koepfli, Benedikt Baeuerle, et al. Plasmonics in future radio communications: Potential and challenges. In *2022 3rd URSI Atlantic and Asia Pacific Radio Science Meeting (AT-AP-RASC)*, pages 1–4. IEEE, 2022.

[30] Ming Li, Scott K Cushing, and Nianqiang Wu. Plasmon-enhanced optical sensors: a review. *Analyst*, 140(2):386–406, 2015.

[31] Briliant Adhi Prabowo, Agnes Purwidyantri, and Kou-Chen Liu. Surface plasmon resonance optical sensor: A review on light source technology. *Biosensors*, 8(3):80, 2018.

[32] Anuj K Sharma, Ankit Kumar Pandey, and Baljinder Kaur. A review of advancements (2007–2017) in plasmonics-based optical fiber sensors. *Optical Fiber Technology*, 43:20–34, 2018.

[33] Jin Tae Kim, Jung Jin Ju, Suntak Park, Min-su Kim, Seung Koo Park, and Myung-Hyun Lee. Chip-to-chip optical interconnect using gold long-range surface plasmon polariton waveguides. *Optics Express*, 16(17):13133–13138, 2008.

[34] Mark L Brongersma, Rashid Zia, and JA Schuller. Plasmonics–the missing link between nanoelectronics and microphotonics. *Applied Physics A*, 89:221–223, 2007.

[35] Jacob B Khurgin and Greg Sun. Injection pumped single mode surface plasmon generators: threshold, linewidth, and coherence. *Optics Express*, 20(14):15309–15325, 2012.

[36] Leland Nordin, Priyanka Petluru, Abhilasha Kamboj, Aaron J Muhowski, and Daniel Wasserman. Ultra-thin plasmonic detectors. *Optica*, 8(12):1545–1551, 2021.

[37] Brian M Wells, Anatoly V Zayats, and Viktor A Podolskiy. Nonlocal optics of plasmonic nanowire metamaterials. *Physical Review B*, 89(3):035111, 2014.

[38] Maryam Farahani, Nosrat Granpayeh, and Mohammad Rezvani. Improved plasmonic splitters and demultiplexers. *Photonics and Nanostructures-Fundamentals and Applications*, 11(2):157–165, 2013.

[39] Darrick E Chang, Anders S Sørensen, Eugene A Demler, and Mikhail D Lukin. A single-photon transistor using nanoscale surface plasmons. *Nature Physics*, 3(11):807–812, 2007.

[40] Nanfang Yu, Jonathan Fan, Qi Jie Wang, Christian Pflügl, Laurent Diehl, Tadataka Edamura, Masamichi Yamanishi, Hirofumi Kan, and Federico Capasso. Small-divergence semiconductor lasers by plasmonic collimation. *Nature Photonics*, 2(9):564–570, 2008.

[41] CA Pfeiffer, EN Economou, and KL Ngai. Surface polaritons in a circularly cylindrical interface: surface plasmons. *Physical Review B*, 10(8):3038, 1974.

[42] Stefan A Maier, Pieter G Kik, Harry A Atwater, Sheffer Meltzer, Elad Harel, Bruce E Koel, and Ari AG Requicha. Local detection of electromagnetic energy transport below the diffraction limit in metal nanoparticle plasmon waveguides. *Nature Materials*, 2(4):229–232, 2003.

[43] Mark L Brongersma, John W Hartman, and Harry A Atwater. Electromagnetic energy transfer and switching in nanoparticle chain arrays below the diffraction limit. *Physical Review B*, 62(24):R16356, 2000.

[44] Stefan A Maier, Mark L Brongersma, Pieter G Kik, and Harry A Atwater. Observation of near-field coupling in metal nanoparticle chains using far-field polarization spectroscopy. *Physical Review B*, 65(19):193408, 2002.

[45] Changjun Min and Georgios Veronis. Absorption switches in metal-dielectric-metal plasmonic waveguides. *Optics Express*, 17(13):10757–10766, 2009.

[46] Rajib Ratan Ghosh and Anuj Dhawan. Integrated non-volatile plasmonic switches based on phase-change-materials and their application to plasmonic logic circuits. *Scientific Reports*, 11(1):18811, 2021.

[47] Rupert F Oulton, Volker J Sorger, Thomas Zentgraf, Ren-Min Ma, Christopher Gladden, Lun Dai, Guy Bartal, and Xiang Zhang. Plasmon lasers at deep subwavelength scale. *Nature*, 461(7264):629–632, 2009.

[48] Jagmeet Singh Sekhon and SS Verma. Plasmonics: the future wave of communication. *Current Science*, 101(4):484–488, 2011.

[49] Juerg Leuthold, C Hoessbacher, S Muehlbrandt, A Melikyan, M Kohl, C Koos, W Freude, V Dolores-Calzadilla, M Smit, I Suarez, et al. Plasmonic communications: light on a wire. *Optics and Photonics News*, 24(5):28–35, 2013.

[50] Stefan A Maier et al. *Plasmonics: fundamentals and applications*, volume 1. Springer, 2007.

[51] Rajan Agrahari, Akhlesh Lakhtakia, and Pradip K Jain. Information carried by a surface-plasmon-polariton wave across a gap. *Journal of Applied Physics*, 124(5), 2018.

[52] Hao Chi Zhang, Shuo Liu, Xiaopeng Shen, Lin Hui Chen, Lianming Li, and Tie Jun Cui. Broadband amplification of spoof surface plasmon polaritons at microwave frequencies. *Laser & Photonics Reviews*, 9(1):83–90, 2015.

[53] Pierre Berini. Long-range surface plasmon polaritons. *Advances in Optics and Photonics*, 1(3):484–588, 2009.

[54] Abdul Rehman, Muhammad Arshad Fiaz, and Muhammad Faryad. Analysis of the scattering of surface plasmon polariton waves from a perfectly conducting circular cylinder. *Plasmonics*, 17(1):361–370, 2022.

[55] Lord Rayleigh. On the dynamical theory of gratings. *Proceedings of the Royal Society of London. Series A, Containing Papers of a Mathematical and Physical Character*, 79(532):399–416, 1907.

[56] Gustav Mie. A contribution to the optics of turbid media, especially colloidal metallic suspensions. *Ann. Phys*, 25(4):377–445, 1908.

[57] George Placzek. *The Rayleigh and Raman scattering*, volume 526. Lawrence Radiation Laboratory, 1959.

[58] David Keun Cheng et al. *Field and wave electromagnetics*. Pearson Education India, 1989.

[59] Constantine A Balanis. *Advanced engineering electromagnetics*. John Wiley & Sons, 2012.

[60] GA Golubenko, Aleksei Sergeevich Svakhin, Vladimir Aleksandrovich Sychugov, and Aleksandr Valentinovich Tishchenko. Total reflection of light from a corrugated surface of a dielectric waveguide. *Soviet Journal of Quantum Electronics*, 15(7):886, 1985.

[61] KO Hill. Photosensitivity in optical fiber waveguides: Application to reflection filter fabrication. *Appl. Phys. Lett.*, 32(10):1035–1037, 1993.

[62] Kenneth N Ogle. *Researches in binocular vision.* WB Saunders, 1950.

[63] Stephen O Rice. Reflection of electromagnetic waves from slightly rough surfaces. *Communications on Pure and Applied Mathematics*, 4(2-3):351–378, 1951.

[64] Metin A Demir and Joel T Johnson. Fourth-and higher-order small-perturbation solution for scattering from dielectric rough surfaces. *JOSA A*, 20(12):2330–2337, 2003.

[65] JM Soto-Crespo, Manuel Nieto-Vesperinas, and AT Friberg. Scattering from slightly rough random surfaces: a detailed study on the validity of the small perturbation method. *JOSA A*, 7(7):1185–1201, 1990.

[66] Li-Xin Guo, Yu Liang, Jie Li, and Zhen-Sen Wu. A high order integral spm for the conducting rough surface scattering with the tapered wave incidence-te case. *Progress In Electromagnetics Research*, 114:333–352, 2011.

[67] A Tabatabaeenejad and M Moghaddam. Bistatic scattering from dielectric structures with two rough boundaries using the small perturbation method. *IEEE Trans. Geosci. Remote Sens*, 44(8):2102–2124, 2006.

[68] MA Fiaz and MA Ashraf. Scattering from pemc rough surface using small perturbation method. *Waves in Random and Complex Media*, 27(1):15–27, 2017.

[69] Saddek Afifi and Richard Dusséaux. Scattering from 2-d perfect electromagnetic conductor rough surface: analysis with the small perturbation method and the small-slope approximation. *IEEE Transactions on Antennas and Propagation*, 66(1):340–346, 2017.

[70] PC Waterman. Scattering by periodic surfaces. *The Journal of the Acoustical Society of America*, 57(4):791–802, 1975.

[71] Shun-Lien Chuang and Jin Au Kong. Scattering of waves from periodic surfaces. *Proceedings of the IEEE*, 69(9):1132–1144, 1981.

[72] SL Chuang and JA Kong. Wave scattering and guidance by dielectric waveguides with periodic surfaces. *JOSA*, 73(5):669–679, 1983.

[73] Leung Tsang, Jin Au Kong, Kung-Hau Ding, and Chi On Ao. *Scattering of electromagnetic waves: numerical simulations*, volume 705. Wiley Online Library, 2001.

[74] C-H Kuo and Mahta Moghaddam. Scattering from multilayer rough surfaces based on the extended boundary condition method and truncated singular value decomposition. *IEEE Transactions on Antennas and Propagation*, 54(10):2917–2929, 2006.

[75] PW Atkins and WILSON AD. Photon scattering from surfaces. *Solid State Surface Sciencee, M. Green, Ed*, 2:153–233, 1973.

[76] GS Agarwal. Relation between waterman's extended boundary condition and the generalized extinction theorem. *Physical Review D*, 14(4):1168, 1976.

[77] SL Chuang and JA Kong. Wave scattering from a periodic dielectric surface for a general angle of incidence. *Radio Science*, 17(3):545–557, 1982.

[78] Shun-Lien Chuang and Richard K Johnson. Acoustic wave scattering from a fluid/solid periodic rough surface. *The Journal of the Acoustical Society of America*, 71(6):1368–1376, 1982.

[79] Constantine A Balanis. *Advanced engineering electromagnetics*. John Wiley & Sons, 2012.

[80] MA Ashraf and AA Rizvi. Electromagnetic scattering from a random cylinder by moments method. *Journal of Electromagnetic Waves and Applications*, 25(4):467–480, 2011.

[81] Yasemin Altuncu, Ali Yapar, and Ibrahim Akduman. On the scattering of electromagnetic waves by bodies buried in a half-space with locally rough interface. *IEEE Transactions on Geoscience and Remote Sensing*, 44(6):1435–1443, 2006.

[82] R Borghi, Fabrizio Frezza, M Santarsiero, Carlo Santini, G Schettini, et al. Numerical study of the reflection of cylindrical waves by a generally reflecting flat surface. *Journal of Electromagnetic Waves and Applications*, 13:27–50, 1999.

[83] R Borghi, Fabrizio Frezza, M Santarsiero, Carlo Santini, and G Schettini. A quadrature algorithm for the evaluation of a 2d radiation integral with a highly oscillating kernel. *Journal of Electromagnetic Waves and Applications*, 14(10):1353–1370, 2000.

[84] R Borghi, F Gori, M Santarsiero, Fabrizio Frezza, and G Schettini. Plane-wave scattering by a perfectly conducting circular cylinder near a plane surface: cylindrical-wave approach. *JOSA A*, 13(3):483–493, 1996.

[85] F Ciambra, Fabrizio Frezza, Lara Pajewski, and G Schettini. A spectral-domain solution for the scattering problem of a circular cylinder buried in a dielectric half-space-abstract. *Journal of Electromagnetic Waves and Applications*, 17(4):607–609, 2003.

[86] Marina Di Vico, Fabrizio Frezza, Lara Pajewski, and Giuseppe Schettini. Scattering by a finite set of perfectly conducting cylinders buried in a dielectric half-space: a spectral-domain solution. *IEEE Transactions on Antennas and Propagation*, 53(2):719–727, 2005.

[87] M Di Vico, Fabrizio Frezza, Lara Pajewski, and G Schettini. Scattering by buried dielectric cylindrical structures. *Radio Science*, 40(06):1–11, 2005.

[88] Lara Pajewski, G Schettini, and Fabrizio Frezza. Cylindrical-wave approach for the electromagnetic scattering problem by buried two-dimensional objects. *Journal of Applied Geophysics*, 67(4):318–326, 2009.

[89] Fabrizio Frezza, Lara Pajewski, Cristina Ponti, Giuseppe Schettini, and Nicola Tedeschi. Electromagnetic scattering by a metallic cylinder buried in a lossy medium with the cylindrical-wave approach. *IEEE Geoscience and Remote Sensing Letters*, 10(1):179–183, 2012.

[90] Cristina Ponti, Massimo Santarsiero, and Giuseppe Schettini. Electromagnetic scattering of a pulsed signal by conducting cylindrical targets embedded in a half-space medium. *IEEE Transactions on Antennas and Propagation*, 65(6):3073–3083, 2017.

[91] Cristina Ponti, Massimo Santarsiero, and Giuseppe Schettini. Time-domain electromagnetic scattering by buried dielectric objects with the cylindrical-wave approach for gpr modelling. *Electronics*, 9(3):421, 2020.

[92] Fabrizio Frezza, Lara Pajewski, C Ponti, and G Schettini. Scattering by conducting cylinders buried in a dielectric layer. In *2009 European Microwave Conference (EuMC)*, pages 1559–1562. IEEE, 2009.

[93] Fabrizio Frezza, Lara Pajewski, Cristina Ponti, and Giuseppe Schettini. Scattering by dielectric circular cylinders in a dielectric slab. *JOSA A*, 27(4):687–695, 2010.

[94] Muhammad Arshad Fiaz, Fabrizio Frezza, Cristina Ponti, and Giuseppe Schettini. Electromagnetic scattering by a circular cylinder buried below a slightly rough gaussian surface. *JOSA A*, 31(1):26–34, 2014.

[95] Fabrizio Frezza, Lara Pajewski, Cristina Ponti, and Giuseppe Schettini. Through-wall electromagnetic scattering by n conducting cylinders. *JOSA A*, 30(8):1632–1639, 2013.

[96] Cristina Ponti and Giuseppe Schettini. The cylindrical wave approach for the electromagnetic scattering by targets behind a wall. *Electronics*, 8(11):1262, 2019.

[97] Muhammad Arshad Fiaz, Fabrizio Frezza, Lara Pajewski, Cristina Ponti, and Giuseppe Schettini. Scattering by a circular cylinder buried under a slightly rough surface: the cylindrical-wave approach. *IEEE Transactions on Antennas and Propagation*, 60(6):2834–2842, 2012.

[98] Cristina Ponti and Stefano Vellucci. Scattering by conducting cylinders below a dielectric layer with a fast noniterative approach. *IEEE Transactions on Microwave Theory and Techniques*, 63(1):30–39, 2014.

[99] F Pincemin, AA Maradudin, AD Boardman, and J-J Greffet. Scattering of a surface plasmon polariton by a surface defect. *Physical Review B*, 50(20):15261, 1994.

[100] Jose A Sánchez-Gil. Coupling, resonance transmission, and tunneling of surface-plasmon polaritons through metallic gratings of finite length. *Physical Review B*, 53(15):10317, 1996.

[101] U Schröter and D Heitmann. Surface-plasmon-enhanced transmission through metallic gratings. *Physical Review B*, 58(23):15419, 1998.

[102] José A Sánchez-Gil and AA Maradudin. Near-field and far-field scattering of surface plasmon polaritons by one-dimensional surface defects. *Physical Review B*, 60(11):8359, 1999.

[103] José A Sánchez-Gil and Alexei A Maradudin. Dynamic near-field calculations of surface-plasmon polariton pulses resonantly scattered at submicron metal defects. *Optics Express*, 12(5):883–894, 2004.

[104] AB Evlyukhin and SI Bozhevolnyi. Point-dipole approximation for surface plasmon polariton scattering: Implications and limitations. *Physical Review B—Condensed Matter and Materials Physics*, 71(13):134304, 2005.

[105] AB Evlyukhin and Sergey Iosiphovich Bozhevolnyi. Applicability conditions for the dipole approximation in the problems of scattering of surface plasmon polaritons. *Journal of Experimental and Theoretical Physics Letters*, 81:218–221, 2005.

[106] K Lance Kelly, Eduardo Coronado, Lin Lin Zhao, and George C Schatz. The optical properties of metal nanoparticles: the influence of size, shape, and dielectric environment. *The Journal of Physical Chemistry B*, 107(3):668–677, 2003.

[107] Jörg P Kottmann, Olivier JF Martin, David R Smith, and Sheldon Schultz. Plasmon resonances of silver nanowires with a nonregular cross section. *Physical Review B*, 64(23):235402, 2001.

[108] Andreas Hohenau, Joachim R Krenn, Gerburg Schider, Harald Ditlbacher, Alfred Leitner, Franz R Aussenegg, and William L Schaich. Optical near-field of multipolar plasmons of rod-shaped gold nanoparticles. *Europhysics Letters*, 69(4):538, 2005.

[109] Andrey B Evlyukhin and Sergey I Bozhevolnyi. Surface plasmon polariton scattering by small ellipsoid particles. *Surface Science*, 590(2-3):173–180, 2005.

[110] Rupert F Oulton, David FP Pile, Yongmin Liu, and Xiang Zhang. Scattering of surface plasmon polaritons at abrupt surface interfaces: Implications for nanoscale cavities. *Physical Review B—Condensed Matter and Materials Physics*, 76(3):035408, 2007.

[111] Sergey I Bozhevolnyi, Valentyn S Volkov, Eloise Devaux, Jean-Yves Laluet, and Thomas W Ebbesen. Channel plasmon subwavelength waveguide components including interferometers and ring resonators. *Nature*, 440(7083):508–511, 2006.

[112] Mark I Stockman. Nanofocusing of optical energy in tapered plasmonic waveguides. *Physical Review Letters*, 93(13):137404, 2004.

[113] Rashid Zia and Mark L Brongersma. Surface plasmon polariton analogue to young's double-slit experiment. *Nature Nanotechnology*, 2(7):426–429, 2007.

[114] Zhaowei Liu, Jennifer M Steele, Hyesog Lee, and Xiang Zhang. Tuning the focus of a plasmonic lens by the incident angle. *Applied Physics Letters*, 88(17), 2006.

[115] Igor I Smolyaninov, David L Mazzoni, Joseph Mait, and Christopher C Davis. Experimental study of surface-plasmon scattering by individual surface defects. *Physical Review B*, 56(3):1601, 1997.

[116] Justin Elser and Viktor A Podolskiy. Scattering-free plasmonic optics with anisotropic metamaterials. *Physical Review Letters*, 100(6):066402, 2008.

[117] Jennifer A Dionne, Luke A Sweatlock, Matthew T Sheldon, A Paul Alivisatos, and Harry A Atwater. Silicon-based plasmonics for on-chip photonics. *IEEE Journal of Selected Topics in Quantum Electronics*, 16(1):295–306, 2010.

[118] CJ Bouwkamp. On sommerfeld's surface wave. *Physical Review*, 80(2):294, 1950.

[119] HM Barlow and J Brown. *Radio Surface Waves Clarendon*. Oxford, 1962.

[120] Allan D Boardman. *Electromagnetic surface modes*. New York: Wiley, 1982.

[121] Jonathan Zenneck. Über die fortpflanzung ebener elektromagnetischer wellen längs einer ebenen leiterfläche und ihre beziehung zur drahtlosen telegraphie, (On the propagation of plane electromagnetic waves along a flat conducting surface and their relationship to wireless telegraphy). *Annalen der Physik*, 328(10):846–866, 1907.

[122] Arnold Sommerfeld. Über die ausbreitung der wellen in der drahtlosen telegraphie, (On the propagation of waves in wireless telegraphy). *Annalen der Physik*, 333(4):665–736, 1909.

[123] David A Hill and James R Wait. On the excitation of the zenneck surface wave over the ground at 10 mhz. In *Annales of Telecommunications*, volume 35, pages 179–182, 1980.

[124] Vladimir Nikolaevich Datsko, Anatolii Andreevich Kopylov, et al. On surface electromagnetic waves. *Physics-Uspekhi*, 51(1):101–102, 2008.

[125] RH Ritchie and HB Eldridge. Optical emission from irradiated foils. i. *Physical Review*, 126(6):1935, 1962.

[126] Stefan A Maier et al. *Plasmonics: fundamentals and applications*, volume 1. Springer, 2007.

[127] M Dragoman and D Dragoman. Plasmonics: Applications to nanoscale terahertz and optical devices. *Progress in Quantum Electronics*, 32(1):1–41, 2008.

[128] Martin G Blaber, Matthew D Arnold, and Michael J Ford. A review of the optical properties of alloys and intermetallics for plasmonics. *Journal of Physics: Condensed Matter*, 22(14):143201, 2010.

[129] John A Polo Jr and Akhlesh Lakhtakia. Surface electromagnetic waves: a review. *Laser & Photonics Reviews*, 5(2):234–246, 2011.

[130] Paul R West, Satoshi Ishii, Gururaj V Naik, Naresh K Emani, Vladimir M Shalaev, and Alexandra Boltasseva. Searching for better plasmonic materials. *Laser & Photonics Reviews*, 4(6):795–808, 2010.

[131] G Borstel, E Schuller, and HJ Falge. Surface phonon polaritons on absorbing crystals. *Physica Status Solidi (b)*, 76(2):759–768, 1976.

[132] RF Wallis. *Surface magnetoplasmons on semiconductors*. Wiley New York, 1982.

[133] SJ Elston and JR Sambles. Surface plasmon-polaritons on an anisotropic substrate. *Journal of Modern Optics*, 37(12):1895–1902, 1990.

[134] Ricardo A Depine and Miriam L Gigli. Excitation of surface plasmons and total absorption of light at the flat boundary between a metal and a uniaxial crystal. *Optics Letters*, 20(21):2243–2245, 1995.

[135] Haiming Wang. Excitation of surface plasmon oscillations at an interface between anisotropic dielectric and metallic media. *Optical Materials*, 4(5):651–656, 1995.

[136] Ricardo A Depine and Miriam L Gigli. Resonant excitation of surface modes at a single flat uniaxial–metal interface. *JOSA A*, 14(2):510–519, 1997.

[137] Ibrahim Abdulhalim. Surface plasmon te and tm waves at the anisotropic film–metal interface. *Journal of Optics A: Pure and Applied Optics*, 11(1):015002, 2008.

[138] John A Polo Jr and Akhlesh Lakhtakia. On the surface plasmon polariton wave at the planar interface of a metal and a chiral sculptured thin film. *Proceedings of the Royal Society A: Mathematical, Physical and Engineering Sciences*, 465(2101):87–107, 2009.

[139] R Haupt and L Wendler. Dispersion and damping properties of plasmon polaritons in superlattice structures ii. semi-infinite superlattice. *Physica Status Solidi (b)*, 142(2):423–435, 1987.

[140] Jorge A Gaspar-Armenta and Francisco Villa. Photonic surface-wave excitation: photonic crystal–metal interface. *JOSA B*, 20(11):2349–2354, 2003.

[141] Ritwick Das and Rajan Jha. On the modal characteristics of surface plasmon polaritons at a metal-bragg interface at optical frequencies. *Applied Optics*, 48(26):4904–4908, 2009.

[142] Yi-Jun Jen, Akhlesh Lakhtakia, Ching-Wei Yu, and Tzu-Yi Chan. Multilayered structures for p-and s-polarized long-range surface-plasmon-polariton propagation. *JOSA A*, 26(12):2600–2606, 2009.

[143] John A Polo Jr and Akhlesh Lakhtakia. Energy flux in a surface-plasmon-polariton wave bound to the planar interface of a metal and a structurally chiral material. *JOSA A*, 26(7):1696–1703, 2009.

[144] GJ Sprokel, R Santo, and JD Swalen. Determination of the surface tilt angle by attenuated total reflection. *Molecular Crystals and Liquid Crystals*, 68(1):29–38, 1981.

[145] GJ Sprokel. The reflectivity of a liquid crystal cell in a surface plasmon experiment. *Molecular Crystals and Liquid Crystals*, 68(1):39–45, 1981.

[146] Jiří Homola and Marek Piliarik. *Surface plasmon resonance (SPR) sensors*. Springer, 2006.

[147] Ibrahim Abdulhalim, Mohammad Zourob, and Akhlesh Lakhtakia. Surface plasmon resonance for biosensing: a mini-review. *Electromagnetics*, 28(3):214–242, 2008.

[148] Tom G Mackay and Akhlesh Lakhtakia. Modeling columnar thin films as platforms for surface–plasmonic–polaritonic optical sensing. *Photonics and Nanostructures-Fundamentals and Applications*, 8(3):140–149, 2010.

[149] DP Pulsifer, A Lakhtakia, et al. Multiple surface plasmon polariton waves. *Electronics letters*, 45(22):1, 2009.

[150] Akhlesh Lakhtakia, Yi-Jun Jen, and Chia-Feng Lin. Multiple trains of same-color surface plasmon-polaritons guided by the planar interface of a metal and a sculptured nematic thin film. part iii: Experimental evidence. *Journal of Nanophotonics*, 3(1):033506, 2009.

[151] WM Robertson and MS May. Surface electromagnetic wave excitation on one-dimensional photonic band-gap arrays. *Applied physics letters*, 74(13):1800–1802, 1999.

[152] Zdzislaw Salamon, H Angus Macleod, and Gordon Tollin. Coupled plasmon-waveguide resonators: a new spectroscopic tool for probing proteolipid film structure and properties. *Biophysical Journal*, 73(5):2791–2797, 1997.

[153] Erwin Kretschmann and Heinz Raether. Radiative decay of non radiative surface plasmons excited by light. *Zeitschrift für Naturforschung A*, 23(12):2135–2136, 1968.

[154] Andreas Otto. Excitation of nonradiative surface plasma waves in silver by the method of frustrated total reflection. *Zeitschrift für Physik A Hadrons and Nuclei*, 216(4):398–410, 1968.

[155] Sophocles J Orfanidis. *Electromagnetic waves and antennas*. Rutgers University New Brunswick, NJ, 2002.

[156] John Moreland, Arnold Adams, and Paul K Hansma. Efficiency of light emission from surface plasmons. *Physical Review B*, 25(4):2297, 1982.

[157] PT Worthing and William L Barnes. Efficient coupling of surface plasmon polaritons to radiation using a bi-grating. *Applied Physics Letters*, 79(19):3035–3037, 2001.

[158] William L Barnes, Alain Dereux, and Thomas W Ebbesen. Surface plasmon subwavelength optics. *Nature*, 424(6950):824–830, 2003.

[159] Paul V Lambeck. Integrated optical sensors for the chemical domain. *Measurement Science and Technology*, 17(8):R93, 2006.

[160] Leung Tsang, Jin Au Kong, Kung-Hau Ding, and Chi On Ao. *Scattering of electromagnetic waves: numerical simulations*. John Wiley & Sons, 2004.

[161] Cristina Ponti and Stefano Vellucci. Scattering by conducting cylinders below a dielectric layer with a fast noniterative approach. *IEEE Transactions on Microwave Theory and Techniques*, 63(1):30–39, 2014.

[162] Ashfaq Ahmad and Muhammad Arshad Fiaz. Scattered field from a pemc cylinder buried below rough interface using extended boundary condition method. *Optik*, 193:162572, 2019.

[163] MA Fiaz, Fabrizio Frezza, Lara Pajewski, C Ponti, and G Schettini. Asymptotic solution for a scattered field by cylindrical objects buried beneath a slightly rough surface. *Near Surface Geophysics*, 11(2):177–184, 2013.

sources:

1 2% match (Faryad, Muhammad. "Propagation and excitation of multiple surface waves.",
Proquest, 2014.)

Faryad, Muhammad. "Propagation and excitation of multiple surface waves.", Proquest, 2014.

2 1% match (Internet from 25-Apr-2024)

https://arcadia.sba.uniroma3.it/bitstream/2307/4076/1/Electromagnetic%20scattering%20by%20cylindrical%20objects%20buried%20
infinite%20medium%20with%20a%20rough%20surface.pdf

3 1% match (student papers from 14-Feb-2020)
Submitted to Higher Education Commission Pakistan on 2020-02-14

4 1% match (Internet from 27-Feb-2022)
https://ebin.pub/optoelectronics-and-photonics-principles-and-practices-9780132151498-
0273774174-9780273774174-0132151499.html

5 1% match (M. Ahmed, M.A. Fiaz, M.A. Ashraf. "Investigation of RCS dependence on
chirality for a chiral cylinder buried below slightly rough surface", AEU - International Journal
of Electronics and Communications, 2016)

M. Ahmed, M.A. Fiaz, M.A. Ashraf. "Investigation of RCS dependence on chirality for a chiral cylinder
buried below slightly rough surface", AEU - International Journal of Electronics and Communications,
2016

6 1% match (Justin Elser, Viktor A. Podolskiy. "Scattering-Free Plasmonic Optics with
Anisotropic Metamaterials", Physical Review Letters, 2008)

Justin Elser, Viktor A. Podolskiy. "Scattering-Free Plasmonic Optics with Anisotropic
Metamaterials", Physical Review Letters, 2008

7 1% match (S. L. Chuang, J. A. Kong. "Wave scattering and guidance by dielectric
waveguides with periodic surfaces", Journal of the Optical Society of America, 1983)

S. L. Chuang, J. A. Kong. "Wave scattering and guidance by dielectric waveguides with
periodic surfaces", Journal of the Optical Society of America, 1983

8 1% match (Shun-Lien Chuang, Jin Au Kong. "Scattering of waves from periodic surfaces",
Proceedings of the IEEE, 1981)

Shun-Lien Chuang, Jin Au Kong. "Scattering of waves from periodic surfaces", Proceedings of
the IEEE, 1981

9 < 1% match (student papers from 27-Jun-2020)
Submitted to Higher Education Commission Pakistan on 2020-06-27

10 < 1% match (student papers from 03-Feb-2020)
Submitted to Higher Education Commission Pakistan on 2020-02-03

11 < 1% match (Internet from 30-Jun-2020)
http://docplayer.net/52453066-Plasmonics-the-future-wave-of-communication.html